

# Reexamination of the magma plumbing system of the Suwolbong tuff ring, Jeju Island, Korea, based on a refined componentry analysis

Sun Young Go<sup>1</sup>, Hyeon-Seon Ahn<sup>2,3</sup>, Ung San Ahn<sup>4</sup>, Jong Ok Jeong<sup>5</sup>, Young Kwan Sohn<sup>6</sup>, and Chang Woo Kwon<sup>1\*</sup>

<sup>1</sup>Volcano Research Group, Geologic Hazards Research Division, Korea Institute of Geoscience and Mineral Resources, Daejeon 34132, Republic of Korea

<sup>2</sup>Quaternary Environment Research Center, Climate Change Response Division, Korea Institute of Geoscience and Mineral Resources, Daejeon 34132, Republic of Korea

<sup>3</sup>Department of Geological Science, Korea National University of Science and Technology (UST), Daejeon 34113, Republic of Korea

<sup>4</sup>World Heritage Office, Jeju Special Self-Governing Provincial Government, Jeju 63341, Republic of Korea

<sup>5</sup>Center for Research Facilities, Gyeongsang National University, Jinju 52828, Republic of Korea

<sup>6</sup>Department of Geology, Gyeongsang National University, Jinju 52828, Republic of Korea

**ABSTRACT:** The Suwolbong tuff ring is a basaltic monogenetic volcano in the Quaternary intraplate volcanic field of Jeju Island, Korea. The tuff ring was formerly interpreted to have had a congested magma plumbing system consisting of multiply-sourced dike complexes, based on stepped and mixed chemical trends of alkaline to sub-alkaline glassy pyroclasts. Microscopic observations, petrological analysis, and componentry analysis of the glassy pyroclasts reveal, however, that some of the glassy pyroclasts in the tuff ring are accidental and inappropriate for interpreting magmatic processes. Juvenile particles are vesicular, alkaline in composition, mainly contain olivine, clinopyroxene, and plagioclase phenocrysts, and comprise about 35 vol% of the deposits. In contrast, accidental particles are non-vesicular, alkaline to subalkaline in composition, less abundant (avg. 8 vol%), and show alteration rims. The accidental particles are interpreted to have been derived from the volcaniclastic layers deposited before the eruption of the Suwolbong tuff ring. When removing the effects of the accidental particles and considering only the geochemical characteristics of the newly defined juvenile particles, the Suwolbong tuff ring is interpreted to have had a rather simple, not necessarily congested, plumbing system fed by independently ascending multiple magma batches. This study shows that the interpretation of the properties of the source magma and the magma plumbing system in monogenetic volcanoes must be performed after clearly distinguishing between juvenile and accidental particles based on rigorous microscopic analysis of pyroclastic materials.

**Key words:** tuff ring, monogenetic volcano, magma plumbing system, tephra componentry, hyaloclastite, Jeju Island

Manuscript received April 2, 2024; Manuscript accepted May 10, 2024

## 1. INTRODUCTION

Tuff rings, tuff cones, and maars are monogenetic volcanoes that erupt only once in their lifetime, with no significant breaks

Editorial responsibility: Youngbeom Cheon

\*Corresponding author:

Chang Woo Kwon

Volcano Research Group, Active Tectonics Research Center, Geologic Hazards Research Division, Korea Institute of Geoscience and Mineral Resources (KIGAM), 124 Gwanhak-ro, Yuseong-gu, Daejeon 34132, Republic of Korea

Tel: +82-10-7922-9690, Fax: +82-42-868-3075, E-mail: cwkwon@kigam.re.kr

©The Association of Korean Geoscience Societies and Springer 2024

in eruptive activity (Smith and Nemeth, 2017). The magma plumbing systems of these volcanoes are generally simple and consist of small volumes (typically < 1 km<sup>3</sup>, commonly < 0.1 km<sup>3</sup>) of individual magmatic batches (Walker, 1993; Smith and Nemeth, 2017). However, some volcanoes have recently been reported to have complex plumbing systems with magma flowing through an upper conduit connected to various geometrically intricate pathways and hydrological systems (Németh et al., 2001; Valentine and Krogh, 2006; Németh and Martin, 2007; Brenna et al., 2011; Valentine et al., 2011). Therefore, the interpretation of the magma plumbing systems of these volcanoes is not always straightforward and needs to be based on carefully analyzed geochemical data of pyroclastic deposits. One of the important obstacles to analysis

is that these volcanoes commonly contain abundant accidental materials in addition to juvenile materials, which were excavated from the substrate associated with diatreme-forming phreatomagmatic activity (Barberi et al., 1989; Valentine and White, 2012; Lefebvre et al., 2013; Valentine et al., 2017; Romero et al., 2022). These volcanoes are characterized by repeated subsurface explosions at various depths, which cause both upward and downward mixing of diatreme-fill by debris jets and subsidence (Lorenz, 1986; Sohn, 1996; White, 1996; White and Houghton, 2000; Ross et al., 2008a, 2008b; White and Ross, 2011; Valentine and White, 2012; Sweeney and Valentine, 2015; Valentine et al., 2017). During this process, accidental materials are fed into the diatreme from the conduit walls and root zones at varying crustal levels and occasionally from the upper mantle (White and Ross, 2011; Valentine et al., 2017). Accidental materials can include particles of various origins, such as fragments of lava, tuff, and basement rocks, depending on the geology of the eruptive site (e.g., Lefebvre et al., 2013; Elliott et al., 2015; Go et al., 2017; Indriyanto et al., 2023). Accidental glass particles can sometimes be mistaken for juvenile materials, leading to misinterpretation of the chemistry of the source magma and the nature of the magma plumbing system. Therefore, it is important to properly distinguish between juvenile and accidental particles before proceeding with chemical analysis.

Suwolbong is a monogenetic basaltic tuff ring on the Quaternary intraplate basaltic volcanic field of Jeju Island (Sohn et al., 1996). Brenna et al. (2011) reported that the glass composition of the Suwolbong tuff ring shows a spectrum between alkaline to mildly subalkaline magmas and interpreted the compositional variations as being formed through a congested plumbing system containing several smaller dikes rather than a single simple plumbing system. We could confirm that the glassy pyroclasts in the tuff ring have alkaline to subalkaline compositions, but also found that they have contrastingly different textural characteristics. It is hardly conceivable that all these chemically and texturally different glassy pyroclasts are juvenile and originated from the same eruption because there are no such cases reported on Jeju Island. Therefore, it is necessary to reveal the origin of the subalkaline and alkaline glass particles, i.e., whether they are both juvenile particles, before interpreting the magma plumbing system. In this study, microscopic textural observations, petrological analysis, and rigorous componentry analysis were conducted to determine the origin of the alkaline and subalkaline glassy pyroclasts in Suwolbong. Then, the eruption process and magma plumbing system of the Suwolbong tuff ring reinterpreted based on the analysis only of juvenile particles.

## 2. GEOLOGICAL SETTING

Jeju is a Quaternary basaltic volcanic field situated on the approximately 100-m-deep Yellow Sea continental shelf off the

southern coast of the Korean Peninsula (Brenna et al., 2015) (Fig. 1). The island was initially produced by widespread hydrovolcanic activity on the continental shelf between ca. 1.88 and 0.5 Ma (Koh, 1997; Koh et al., 2013). The activity produced a subsurface hydrovolcanic succession named the Seoguipo Formation (Fig. 1b). Later volcanic activity was dominated by lava effusion, which produced a gently sloping lava shield and a 1950 m-high central peak (Mt. Hallasan) dotted with hundreds of volcanic cones (Sohn and Park, 2004; Sohn et al., 2008) (Fig. 1c). The lava composition varies from alkali basalt to trachyte and subalkali basalt to andesite (Park et al., 1999). Several tuff rings and tuff cones were produced on top of the lava shield by the hydrovolcanic activity in the coastal regions in the Late Pleistocene and Holocene (Sohn et al., 2002; Cheong et al., 2007).

Suwolbong is a low-relief tuff ring located at the western margin of the island (Sohn and Chough, 1989) (Fig. 1d). The age of the tuff ring is  $18.3 \pm 0.7$  ka and  $18.6 \pm 0.9$  ka by OSL dating of the accidental quartz grains in the tuff (Cheong et al., 2007). Recent  $^{14}\text{C}$  dating of the uppermost part of the Gosan Formation, which is a clayey sedimentary formation beneath the tuff ring, suggests that Suwolbong is younger than at least  $17,140 \pm 300$  calibrated yr BP (Lim et al., 2015). These ages suggest that the eruption of Suwolbong occurred under subaerial conditions during the LGM when the sea level was lowered by 100 to 130 m than at present (Cheong et al., 2007; Lim et al., 2015). Currently, the crater of the Suwolbong tuff ring is submerged in the sea, and the tuff ring, ca. 70 m thick, provides excellent and continuous sea cliff exposures. The tuff ring deposits show lateral facies transitions that begin with massive or crudely stratified lapilli tuff in the most proximal part and transform downcurrent into planar-stratified, undulatory-stratified, climbing megaripple-bedded (lapilli) tuff, and thinly and planar-stratified tuff, depending on flow regimes (Sohn and Chough, 1989). The vertical facies change in the tuff ring suggests an overall decrease in the abundance of external water and fluctuations in the rate of magma rise (Sohn and Chough, 1989). Brenna et al. (2011) conducted detailed geochemical investigations of glassy pyroclasts in Suwolbong using whole-rock selected major (X-ray fluorescence) and trace-element (laser ablation ion coupled plasma mass spectrometry) analyses. They showed that the glassy pyroclasts of Suwolbong have a chemical spectrum between alkali to mildly sub-alkali magmas, indicating some mixing and interaction between magmas from different sources. They proposed that the eruption of Suwolbong was fed by several magma pulses without eruption breaks and that the vents opened at a new location, generating an asymmetric tuff ring. The magma plumbing system was interpreted to have been congested, probably with temporary storage and stagnation of magma in the shallow dike/sill complexes (Brenna et al., 2011).

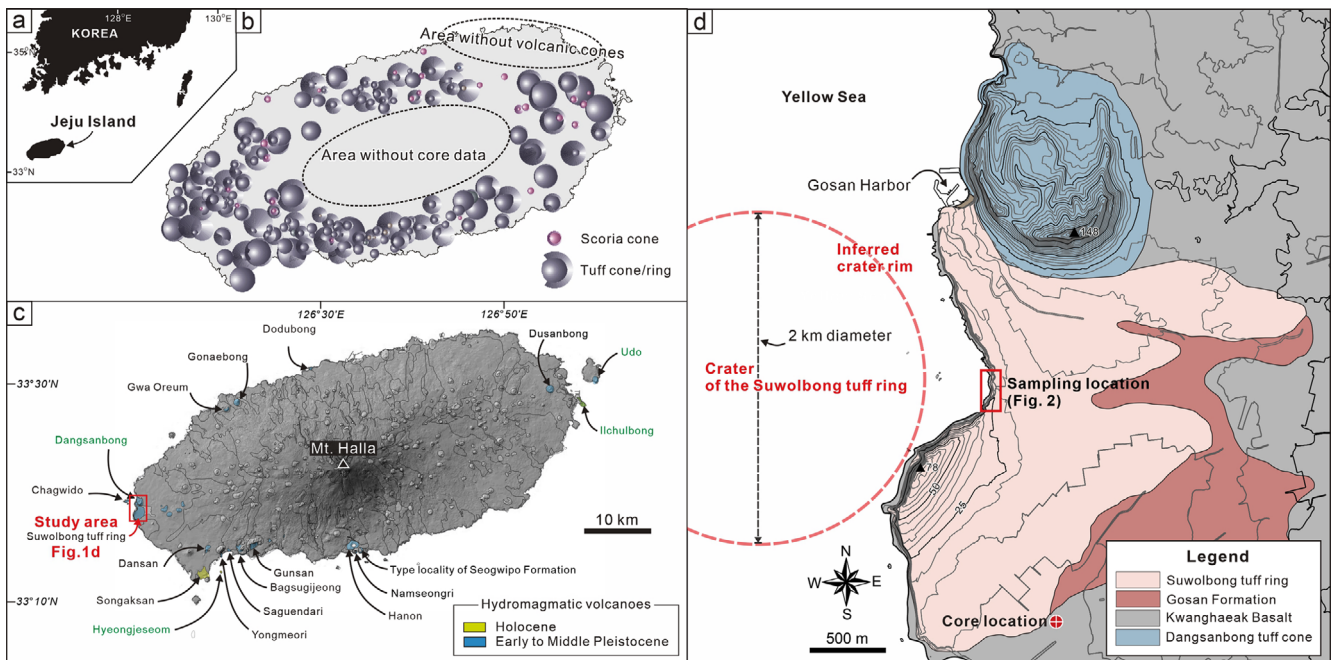


**Fig. 1.** Location and geology of the study area. (a) Location of Jeju Island. (b) Distribution of subsurface tuff cone, ring, and scoria cones beneath the lavas based on the compilation of core data from approximately 1,400 boreholes (modified after Jeon et al., 2022). The crater diameter of each volcano was determined based on the correlation of adjacent cores. (c) Distribution of surficial hydromagmatic volcanoes with the location of the study area (modified after Park et al., 2000). Black names indicate the tuff rings, and green names indicate the tuff cones. (d) Geological and topographic map of and around the Suwolbong tuff ring (modified after Woo et al., 2013). The topographic contours are in meters. The red circle indicates the core location. The dashed circle indicates an eruption center, inferred from data on the anisotropy of magnetic susceptibility on pyroclastic deposits of the Suwolbong tuff ring (Cho et al., 2021).

### 3. METHODS AND MATERIALS

The Suwolbong tuff ring contains partially preserved rim beds whose inferred vents lie approximately 1 km seaward of the coastline (Fig. 1d). A total of 18 samples were collected from a medial location, approximately 700 m away from the eruption

center of the tuff ring (Fig. 2), where sampling of the whole sequence, approximately 22 m thick, was possible. The deposits comprise mostly thin and crudely bedded tuff/lapilli tuff, low-relief undulatory bedded tuff/lapilli tuff, and disorganized tuff breccia with bedding sags (Fig. 2). These features indicate that all units were mainly emplaced by pyroclastic surges and associated

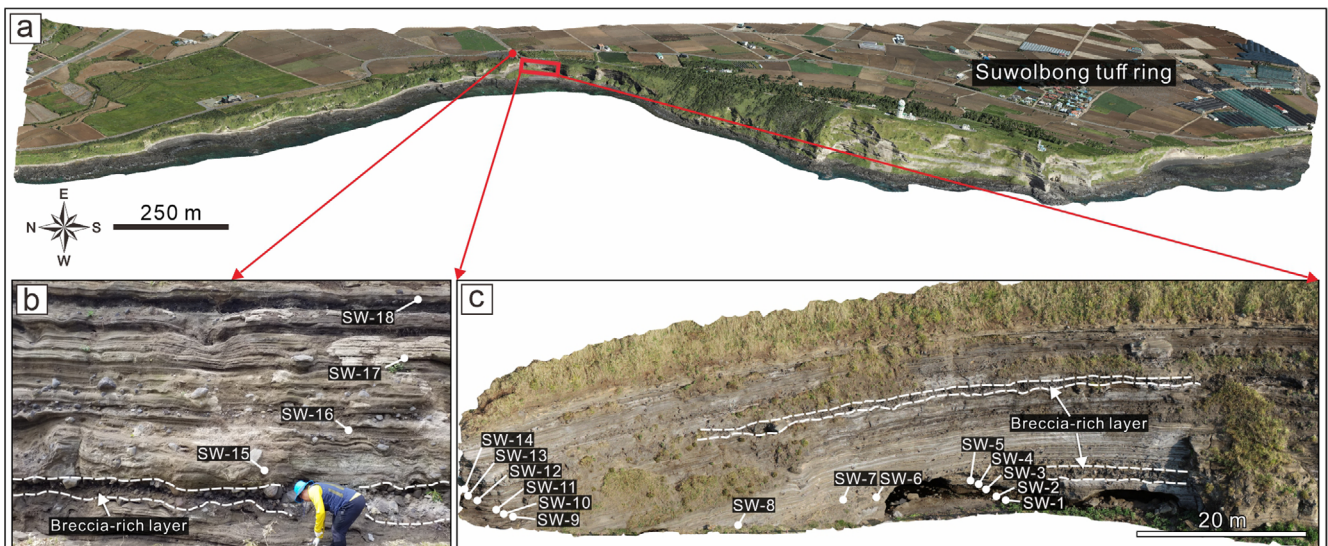


**Fig. 2.** Exposure of the tuff ring along the coast with the sampling locations. (a, c) 3D model of the exposure of the tuff ring, which was built by combining hundreds of images taken with a drone. (b) Outcrop photograph of the upper part of the medial deposits of the tuff ring.

fallouts (Chough and Sohn, 1990). Two breccia units with abundant bedding sags, emplaced by ballistic falls, are intercalated in the lapilli tuff/tuff sequence (Sohn and Chough, 1989).

The micro-textures and chemical compositions of the tuff samples were analyzed. Backscattered electron (BSE) images were obtained from the thin sections using a field-emission electron probe microanalyzer (Model JEOL JXA-8530F Plus, Jeol) equipped with wavelength dispersive spectroscopy (EPMA-WDS) at the Center for Research Facilities of Gyeongsang National University. The instrument was operated at an accelerating voltage of 15 kV and currents ranging between 5 and 10 nA, depending on the beam diameters (5 or 10  $\mu\text{m}$ ). Standards supplied by JEOL were used for the analysis of the major elements. Diopside was used for Mg and Si, K-feldspar for K, kyanite for Al, albite for Na, ilmenite for Fe and Ti, garnet for Mn, wollastonite for Ca, and

synthetic InP for P. To prevent alkali (Na and K) loss, the glass parts were analyzed for 5 s for Na and K and 10 s for the other elements.

To quantify the microtextural features of the Suwolbong pyroclastic deposits, BSE images were analyzed using the ImageJ software (<https://imagej.nih.gov/ij/>) to measure componentry, vesicle size, and vesicularity. Componentry analysis used five images ( $\times 40$ ) from each thin section, with additional higher-magnification images for each sample; over 400 grains with a size of approximately 2–4 phi were analyzed.

Since the 1960s, more than 5,000 groundwater wells have been drilled throughout Jeju Island, revealing its hydrology, subsurface stratigraphy, and lithology (Hahn et al., 1997; Koh, 1997; Sohn and Park, 2004; Won et al., 2005, 2006; Sohn et al., 2008; Koh et al., 2013; Mair et al., 2013; Jeon et al., 2022). Based on geological

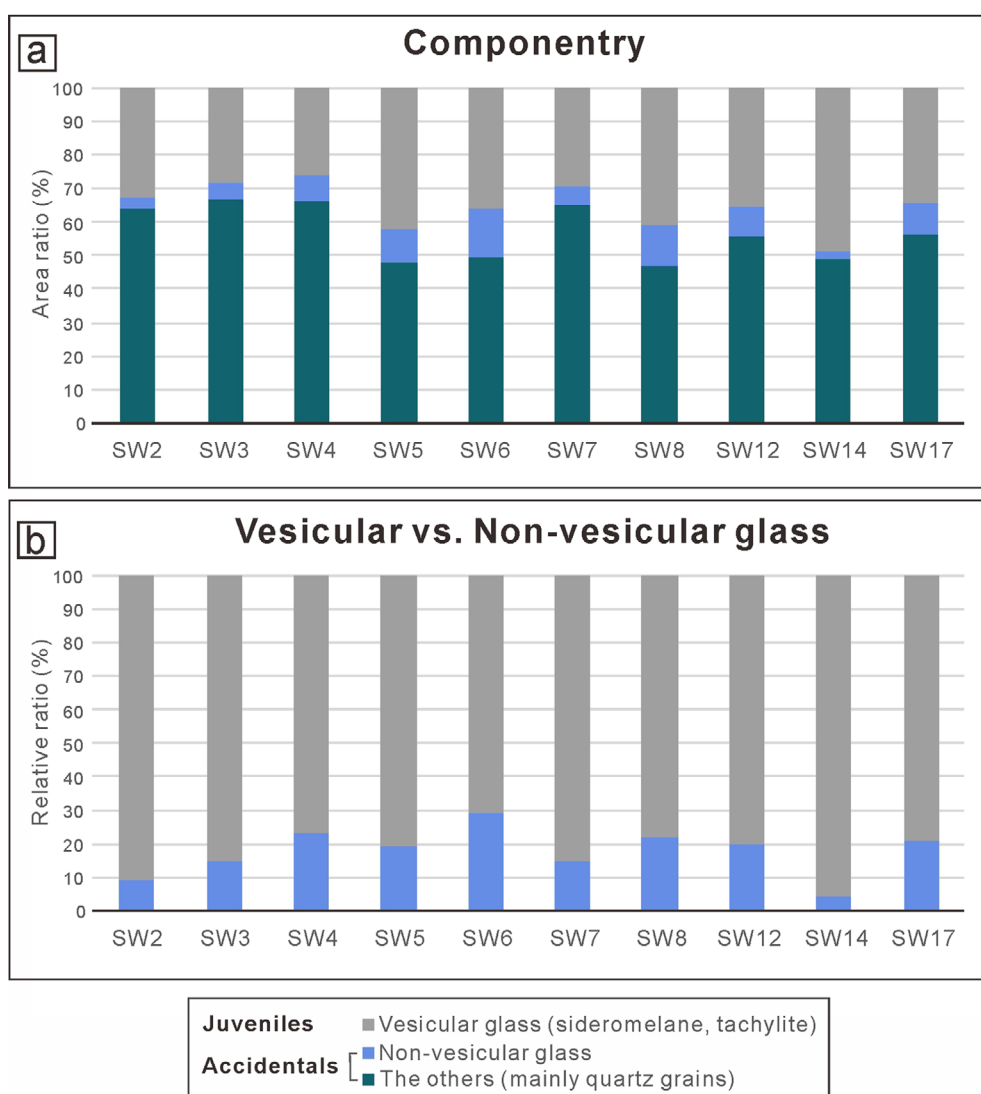


**Fig. 3.** Area ratio of components in the pyroclastic deposits at Suwolbong. (a) Vertical variation in componentry in Suwolbong tuff based on the area ratio analysis of BSE images. (b) Variation of the proportion of vesicular vs. non-vesicular glass. BSE images were analyzed using the Image J™ image-analysis software.

logging data from groundwater level observation wells in the western parts of Jeju Island, the subsurface stratigraphy of the Suwolbong tuff ring was identified. The geochemical and microtexture analyses of tuff block samples derived from the Seoguipo Formation were conducted to determine the features of the old volcaniclastic materials. Based on the results of these analyses, a componentry analysis was performed on the Suwolbong tuff ring samples. For geochemical analysis of the glass, only sideromelane was selected from the pyroclasts.

#### 4. MICROSCOPIC FEATURES AND GEOCHEMICAL CHARACTERISTICS OF GLASSY PYROCLASTS

##### 4.1. Vesicular Glassy Pyroclasts

Componentry analysis shows that vesicular glass particles in each sample ranged between 26 and 48 vol% with an average of 35 vol% (Fig. 3a). These pyroclasts (Fig. 4) contain vesicles of various shapes in an alkaline groundmass. They are a few micrometers to a few millimeters in size, and some fine ash particles occur as a coat on larger particles (Fig. 4a, b). The vesicles are circular to irregular in shape and are randomly distributed within the glass particles. The diameters of the vesicles range from a few micrometers

to one millimeter. The interior of the vesicles and edges of the glass particles are clean without secondary mineral growth. The vesicularity of the glass, calculated from the BSE images of each sample, ranges between 4% and 15% (Fig. 5). The vesicularity shows an overall upward-decreasing trend with two peaks in the breccia-rich layers (Fig. 5). The vesicular glass particles predominantly contain euhedral to subhedral crystals of olivine,

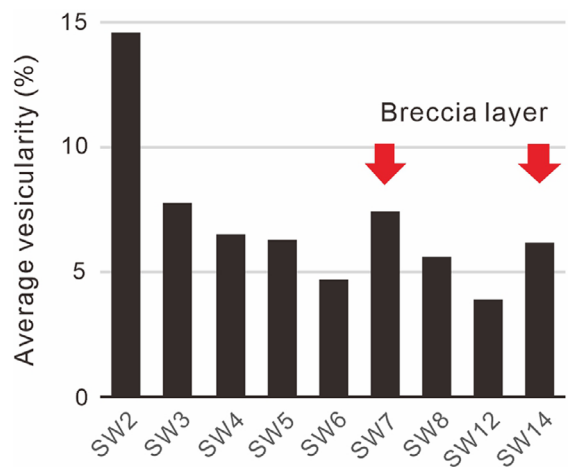


**Fig. 5.** Approximated vesicularity based on the area ratio analysis of gas bubbles in SEM-BSE images using the image J program.

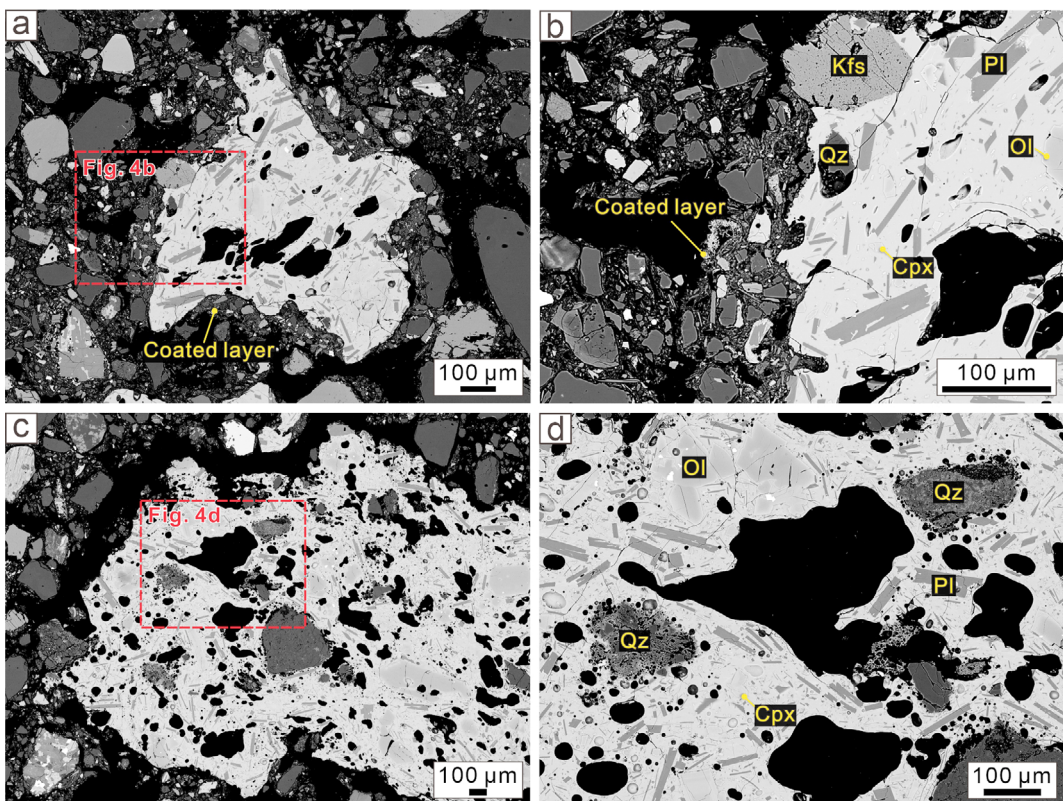


**Fig. 4.** Back-scattered electron (BSE) images of vesicular glass, showing vesicles of various shapes and groundmass of alkaline composition and some quartz and K-feldspar grains derived from surrounding wall rocks. Cpx: clinopyroxene, Ol: olivine, Pl: plagioclase, Kfs: K-feldspar, and Qz: quartz.

clinopyroxene, and plagioclase in the glassy groundmass. The olivine crystals have diameters ranging from tens to hundreds of micrometers and a resorption texture. The plagioclase crystals have acicular and skeletal shapes, mainly  $< 100 \mu\text{m}$ . Clinopyroxene crystals are very fine-grained and several to tens of micrometers in size. Some vesicular glass particles captured considerable amounts of detrital quartz grains and rare K-feldspar in the groundmass and vesicles (Fig. 4b, d). Quartz crystals often show internal fractures and are variably fragmented into pieces surrounded by vesicles several micrometers in size (Fig. 4d).

EPMA point analysis reveals that the vesicular glassy pyroclasts have a total alkali content of 5.2–7.4 wt% and a  $\text{SiO}_2$  content of 45.8–51.5 wt%, which corresponds to the alkaline series of trachybasalt to basaltic trachyandesite in the TAS diagram ( $\text{SiO}_2$  vs.  $\text{Na}_2\text{O} + \text{K}_2\text{O}$ ) (Table 1, Fig. 6a). The  $\text{MgO}$  values of the vesicular glassy pyroclasts have a relatively wide range at the  $\text{SiO}_2$  content of about 47–48 wt%. This implies that the particles were not formed by fractionation from a single magma but originated from multiple magma batches. The  $\text{Mg}^{\#}$  ( $100 * [\text{Mg}^{2+}] / [\text{Mg}^{2+} + \text{Fe}^{2+}]$ ) values of the microlite-free glassy groundmass of the pyroclasts from each sample range from 32 to 50 (Fig. 7). Two samples (SW7 and SW14) collected from the breccia layers have significantly higher  $\text{Mg}^{\#}$  values than the underlying samples. The notably high  $\text{Mg}^{\#}$  values at the bottom and in the middle suggest that there were at least three magma batches with different thermal histories during the Suwolbong tuff ring eruption (Helz and Thornber, 1987; Luhr, 2001; Johnson et al., 2008; Del Gaudio et al., 2010; Johnson et al., 2010). The occurrence of glassy pyroclasts with either high or low values of  $\text{Mg}^{\#}$ s in the same depositional units indicates that there might have been mixing of pyroclasts from different magma sources in the diatreme (Go et al., 2017). However, no evidence of magma mixing within the dike or conduit, such as reverse zoning in olivine crystals or intermediate  $\text{Mg}^{\#}$ s, is found in contrast to the case of the Songaksan tuff ring (Ahn et al., 2015; Go et al., 2017).

#### 4.2. Non-vesicular Glassy Pyroclasts

The componentry analysis shows that the tuff specimens contain 52 to 74 vol% accidental materials, mostly comprising detrital quartz grains (Fig. 3a). The content of non-vesicular glass particles in each sample ranged between 2 and 15 vol% with an average of 8 vol%. The relative proportions of non-vesicular glass particles to vesicular glass particles ranged from 5 to 29% (Fig. 3b). These pyroclasts (Fig. 8) are non- to very poorly vesicular and have a groundmass with an alkaline to subalkaline composition. They generally range from hundreds of micrometers to a few millimeters in size in most specimens, but are over a few centimeters in size in some specimens. They are characterized by a vesicularity

index ranging between 0 and 5% (Houghton and Wilson, 1989), and no vertical changes are observed. Rarely, the vesicles are generally circular or elliptical and larger than  $100 \mu\text{m}$ . The glass particles commonly display well-developed alteration rims around the vesicles and outer edges of the particles (Fig. 8a, b). The alteration rims are uneven with an irregular thickness on the surface and display oscillatory zoning of the smectite (Fig. 8b). A thin zone of leached glass is observed at the interface between the alteration rim and glass. The non-vesicular glass particles mainly contain euhedral to subhedral olivine and plagioclase crystals in the glassy groundmass. The olivine crystals have diameters ranging from tens to hundreds of micrometers and a resorption texture. Plagioclase crystals have tabular and acicular shapes, ranging from tens to hundreds of micrometers in size. In contrast to vesicular glass, they do not contain detrital grains of quartz and K-feldspar.

The EPMA point analysis shows that the non-vesicular glassy pyroclasts have a total alkali content of 2.7–5.5 wt% and a  $\text{SiO}_2$  content of 48.5–55.3 wt%, indicating an alkaline to sub-alkaline series of trachybasalt to basaltic andesite (Table 2, Fig. 6a). The non-vesicular glass is characterized by higher  $\text{SiO}_2$  values and lower  $\text{Al}_2\text{O}_3$ ,  $\text{K}_2\text{O}$ , and  $\text{Na}_2\text{O}$  contents than the vesicular glass (Fig. 6c–e).

The non-vesicular glass can be subdivided into two groups based on crystal size. Group A particles (Fig. 8c) are characterized by lower crystal number density and smaller (mostly  $< 100 \mu\text{m}$  and occasionally  $200 \mu\text{m}$  on the long axis) phenocrysts of plagioclase and olivine than Group B particles (Fig. 8d) (mostly  $> 100 \mu\text{m}$  on the long axis). The two groups also differ in their geochemical compositions. Group A particles, which have a significantly smaller crystal size, have a higher  $\text{SiO}_2$  value and lower alkali content, and are plotted near the boundary between the tholeiitic series and the calc-alkaline series on the  $\text{K}_2\text{O}$  vs.  $\text{SiO}_2$  diagram (Fig. 6b). On the other hand, Group B particles contain relatively low  $\text{SiO}_2$  and high alkalis and are plotted mainly in the region of the high-K calc-alkaline series and some shoshonitic series on the diagram. The two groups are plotted in distinctly different areas in the graph, with no overlapping areas (Fig. 6b).

### 5. SUBSURFACE STRATIGRAPHY AND SOURCES OF ACCIDENTAL MATERIALS

The subsurface stratigraphy was identified based on graphic logging data from a borehole (Gosan) drilled at an elevation of 8.0 m near the Suwolbong tuff ring (Lee, 2008) (Figs. 1 and 9a). Sampling and direct observations of the core were not possible because the core was discarded after coring. The Suwolbong tuff ring is underlain by the Gosan Formation, which consists of approximately 85 cm-thick silty sediments (Lim et al., 2015).

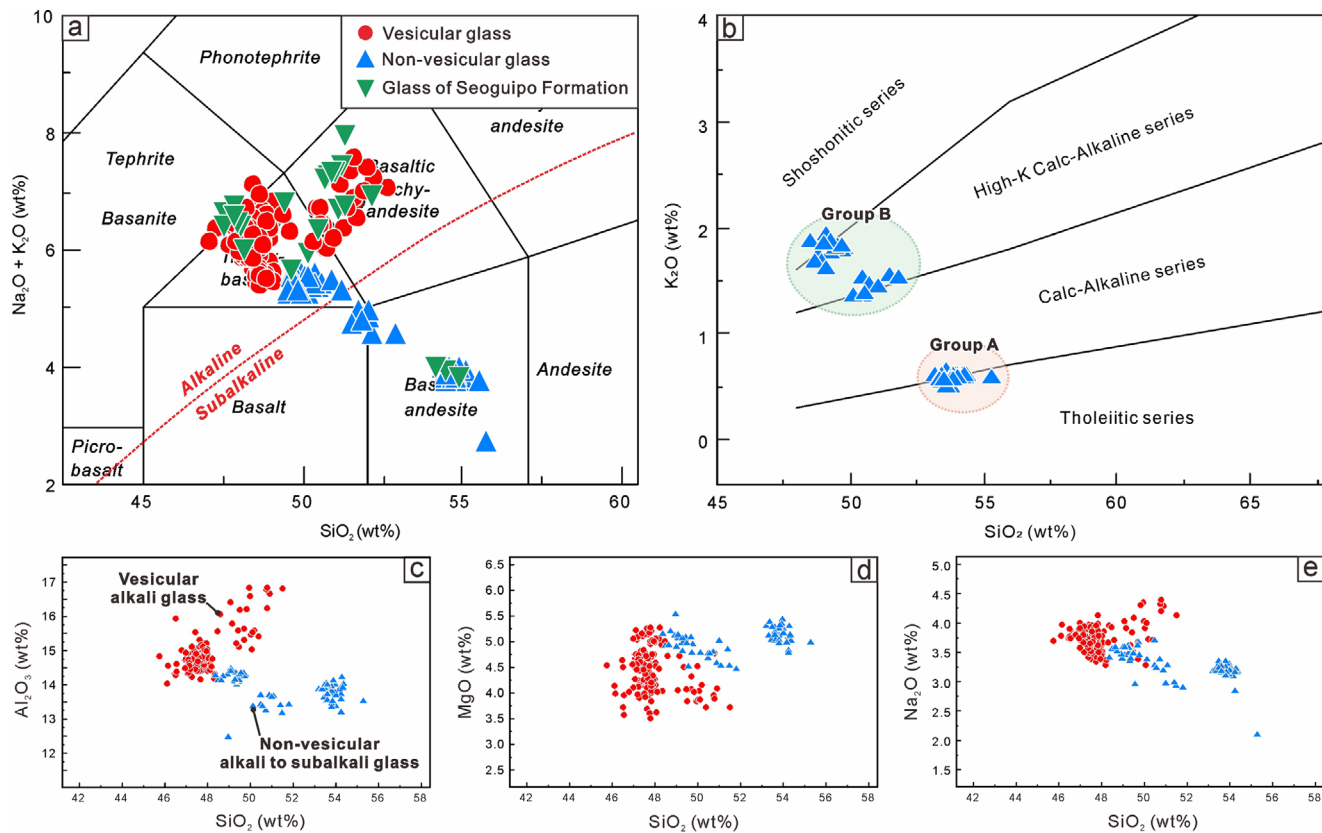


**Fig. 6.** Petrochemical characteristics of the Suwolbong basaltic glass. (a) Total alkali-silica diagram showing the glass compositions of the two distinctive domains. (b–e) Variation diagrams of major element oxides vs.  $\text{SiO}_2$  (in wt%). The non-vesicular glass (blue triangles) shows the two groups with different types in  $\text{K}_2\text{O}$  composition.

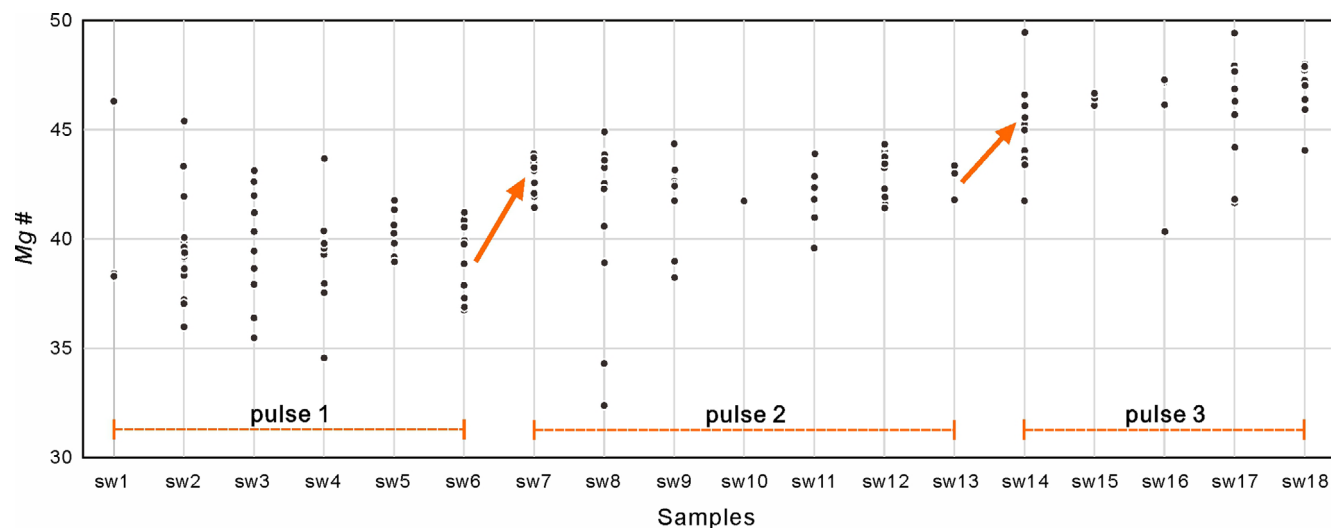


**Fig. 7.** Variations of the magnesium number (Mg#) of the glassy groundmass of sideromelane grains of the vesicular glass, suggesting three magma pulses. The first pulse is for samples SW1–SW6, second pulse is for samples SW7–SW13, and third pulse is for SW14–SW18.

Although the Gosan Formation was not identified in the borehole data, it was confirmed by the outcrop that the Suwolbong tuff ring directly overlies the thin silty sediment of the Gosan Formation (Lim et al., 2015). The Gosan Formation is underlain by pahoehoe

lava flows, approximately 48 m thick, which predominantly contain tabular feldspar and olivine phenocrysts. The lavas correspond to tholeiitic basalts, a type of non-alkaline magma series (Koh et al., 2013). The lavas are underlain by sand- to

**Table 1.** Major element composition of glassy groundmass of vesicular sideromelane grains in the Suwolbong tuff samples

Sample no.	ID	SiO <sub>2</sub>	TiO <sub>2</sub>	Al <sub>2</sub> O <sub>3</sub>	FeO*	Cr <sub>2</sub> O <sub>3</sub>	MnO	MgO	CaO	Na <sub>2</sub> O	K <sub>2</sub> O	P <sub>2</sub> O <sub>5</sub>	Total	Mg#
SW1	VS-1	47.40	3.57	14.73	11.19	–	0.18	3.92	9.36	3.96	2.56	0.66	97.51	38.41
	VS-2	47.72	4.33	14.13	12.21	–	0.12	4.25	9.20	3.53	2.61	0.70	98.80	38.29
	VS-3	48.61	2.63	16.04	9.73	0.06	0.10	4.71	9.18	3.69	2.45	0.77	97.97	46.30
SW2	VS-4	48.11	3.95	14.62	11.13	0.02	0.14	4.14	9.54	3.85	2.40	0.83	98.73	39.89
	VS-5	47.86	3.76	15.03	11.31	0.01	0.17	4.25	9.50	3.98	2.43	0.70	98.98	40.14
	VS-6	48.02	3.81	14.40	11.58	–	0.16	4.17	9.48	3.54	2.53	0.78	98.46	39.11
	VS-7	47.66	3.77	14.67	11.26	–	0.22	4.07	9.15	3.85	2.58	0.67	97.88	39.19
	VS-8	48.06	3.67	14.87	11.40	–	0.20	4.15	9.45	3.50	2.39	0.70	98.40	39.33
	VS-9	47.71	3.84	15.09	11.00	–	0.17	4.13	9.52	3.74	2.30	0.72	98.22	40.07
	VS-10	47.68	4.02	14.65	11.77	0.06	0.15	3.92	9.26	3.78	2.69	0.70	98.67	37.22
	VS-11	47.84	3.69	15.02	11.60	–	0.13	3.82	8.84	4.11	2.84	0.70	98.59	37.01
	VS-12	47.93	4.09	15.05	11.27	0.03	0.15	4.15	9.59	3.53	2.42	0.70	98.91	39.63
	VS-13	47.58	3.50	14.62	11.21	–	0.21	4.09	9.45	3.62	2.42	0.73	97.42	39.37
	VS-14	47.87	3.85	14.55	11.44	0.01	0.13	3.99	9.48	3.45	2.54	0.70	98.02	38.33
	VS-15	46.56	4.15	14.27	11.76	0.01	0.15	3.71	8.47	3.76	2.46	0.74	96.03	35.98
	VS-16	46.58	4.26	14.58	11.96	0.00	0.16	3.95	8.81	3.72	2.42	0.67	97.12	37.05
	VS-17	48.36	3.35	14.15	10.56	0.05	0.17	4.93	9.68	3.65	1.68	0.49	97.07	45.40
	VS-18	49.53	2.78	16.16	9.45	0.01	0.17	3.83	7.16	4.08	2.73	0.77	96.66	41.94
	VS-19	47.03	4.24	14.95	11.59	0.02	0.11	4.09	8.90	3.99	2.28	0.70	97.89	38.64
	VS-20	49.98	2.31	16.81	8.91	–	0.10	3.82	7.13	4.33	2.77	0.71	96.88	43.32
SW3	VS-21	47.32	3.69	14.85	11.29	0.04	0.13	4.13	9.63	3.64	2.41	0.69	97.81	39.44
	VS-22	47.46	3.43	15.51	11.13	–	0.19	3.93	9.95	3.82	2.22	0.64	98.28	38.65
	VS-23	47.66	4.10	14.46	11.43	–	0.23	3.67	8.81	3.83	2.72	0.80	97.69	36.39
	VS-24	47.33	3.78	14.57	10.96	–	0.14	4.16	9.63	3.93	2.39	0.81	97.71	40.33
	VS-25	47.87	3.42	14.89	10.90	0.02	0.22	4.13	9.50	3.62	2.40	0.77	97.74	40.34
	VS-26	49.50	3.02	15.08	10.33	0.02	0.12	4.07	8.46	3.51	2.69	0.81	97.60	41.22
	VS-27	50.10	3.06	15.02	10.23	–	0.17	4.02	8.78	3.27	2.76	0.71	98.11	41.20
	VS-28	46.82	3.86	14.98	11.71	0.02	0.16	4.02	8.88	3.78	2.39	0.76	97.39	37.93
	VS-29	46.58	4.03	14.36	11.56	0.01	0.22	3.57	9.05	3.87	2.57	0.67	96.47	35.48
	VS-30	50.06	2.74	15.45	9.50	–	0.18	3.86	7.97	3.90	2.38	0.65	96.69	41.98
	VS-31	47.31	3.90	15.08	10.60	–	0.16	4.42	8.31	3.66	2.44	0.71	96.59	42.62
	VS-32	49.09	2.91	16.39	9.48	–	0.15	4.04	7.98	4.02	2.44	0.69	97.18	43.13
	VS-33	50.44	2.96	15.38	10.14	0.01	0.12	3.71	7.57	3.69	2.96	0.76	97.72	39.45
SW4	VS-34	50.24	2.83	15.55	9.53	0.00	0.10	4.15	8.67	3.71	2.50	0.66	97.95	43.68
	VS-35	47.39	4.04	14.42	11.68	–	0.18	3.94	9.22	3.79	2.60	0.72	97.96	37.54
	VS-36	47.57	3.83	14.50	11.30	–	0.19	4.10	9.47	3.95	2.34	0.77	98.02	39.29
	VS-37	47.53	3.97	14.64	11.59	–	0.11	3.98	9.43	3.77	2.48	0.74	98.22	37.97
	VS-38	47.77	4.15	14.58	12.11	0.03	0.17	3.59	9.18	3.60	2.68	0.75	98.60	34.56
	VS-39	47.26	3.85	14.64	11.39	–	0.18	4.22	9.56	3.83	2.46	0.64	98.03	39.75
	VS-40	47.60	3.95	14.87	11.48	0.01	0.15	4.25	9.48	3.86	2.37	0.72	98.73	39.76
	VS-41	47.49	3.67	14.66	11.41	0.04	0.20	4.25	9.57	3.78	2.52	0.60	98.19	39.88
	VS-42	47.29	3.54	14.88	11.26	–	0.19	4.14	9.56	3.73	2.38	0.68	97.64	39.57
	VS-43	47.74	3.76	14.40	11.88	0.01	0.18	4.41	9.47	3.78	2.38	0.72	98.72	39.80
	VS-44	47.31	3.61	14.21	10.24	0.02	0.20	3.89	9.35	3.82	2.67	0.79	96.10	40.37

**Table 1.** (continued)

Sample no.	ID	SiO <sub>2</sub>	TiO <sub>2</sub>	Al <sub>2</sub> O <sub>3</sub>	FeO*	Cr <sub>2</sub> O <sub>3</sub>	MnO	MgO	CaO	Na <sub>2</sub> O	K <sub>2</sub> O	P <sub>2</sub> O <sub>5</sub>	Total	Mg#
SW5	VS-45	47.51	3.76	14.89	11.00	0.03	0.16	4.21	9.74	3.78	2.34	0.75	98.17	40.55
	VS-46	47.74	3.58	14.79	11.02	0.02	0.16	4.23	9.31	3.74	2.52	0.73	97.82	40.64
	VS-47	47.49	3.57	14.88	10.73	–	0.12	4.25	9.68	3.91	2.45	0.74	97.82	41.34
	VS-48	47.92	3.78	14.81	11.60	0.02	0.16	4.19	9.56	3.82	2.51	0.67	99.03	39.17
	VS-49	48.01	3.72	14.91	10.58	–	0.15	4.26	9.63	3.79	2.38	0.71	98.13	41.76
	VS-50	47.70	3.78	15.11	11.20	–	0.23	4.16	9.70	3.81	2.29	0.71	98.69	39.80
	VS-51	47.83	3.59	15.19	11.22	0.01	0.15	4.24	9.60	3.58	2.47	0.69	98.58	40.26
	VS-52	47.99	3.51	14.97	11.29	–	0.20	4.05	9.52	3.67	2.44	0.75	98.39	38.96
SW6	VS-53	47.65	3.61	15.28	10.54	–	0.15	4.08	9.63	3.89	2.46	0.67	97.97	40.85
	VS-54	47.95	3.64	14.73	11.10	0.02	0.24	4.14	9.83	3.81	2.37	0.69	98.52	39.93
	VS-55	48.37	3.60	14.29	11.27	–	0.23	4.02	9.23	3.94	2.72	0.77	98.42	38.87
	VS-56	47.85	3.50	14.79	11.06	–	0.16	4.35	9.86	3.85	2.29	0.72	98.43	41.21
	VS-57	47.93	3.69	14.77	11.46	–	0.12	4.25	9.78	3.73	2.51	0.64	98.88	39.76
	VS-58	47.59	3.79	14.81	11.41	0.01	0.17	3.90	9.62	3.68	2.43	0.73	98.11	37.88
	VS-59	47.96	3.67	14.78	11.30	0.02	0.18	4.32	9.88	3.76	2.30	0.64	98.80	40.55
	VS-60	46.14	4.24	14.02	12.67	0.01	0.22	4.13	9.37	3.77	2.41	0.61	97.57	36.74
	VS-61	47.21	3.87	14.70	12.08	0.05	0.13	3.96	9.50	3.92	2.32	0.65	98.39	36.88
	VS-62	46.17	3.60	14.54	11.93	0.01	0.15	3.98	9.43	3.96	2.37	0.61	96.75	37.30
SW7	VS-63	47.65	3.30	14.77	10.78	0.03	0.12	4.67	10.37	3.74	2.17	0.60	98.19	43.55
	VS-64	47.83	3.59	15.04	10.93	–	0.14	4.56	10.16	3.65	2.18	0.64	98.72	42.64
	VS-65	47.41	3.53	14.85	10.99	–	0.17	4.56	10.20	3.70	2.27	0.59	98.26	42.50
	VS-66	47.97	3.43	15.18	10.80	0.02	0.16	4.74	10.35	3.68	2.24	0.72	99.29	43.91
	VS-67	48.06	3.29	14.80	10.77	–	0.16	4.58	10.24	3.63	2.20	0.65	98.37	43.12
	VS-68	47.71	3.46	14.90	10.60	–	0.13	4.58	10.32	3.78	2.14	0.70	98.33	43.51
	VS-69	47.58	3.36	14.99	10.66	–	0.18	4.65	10.25	3.48	2.10	0.56	97.80	43.72
	VS-70	47.55	3.36	14.81	10.69	0.02	0.18	4.57	10.37	3.46	2.22	0.60	97.83	43.26
	VS-71	47.65	3.26	14.87	10.85	–	0.11	4.51	10.34	3.75	2.15	0.66	98.16	42.57
	VS-72	47.49	3.39	14.89	10.95	–	0.17	4.44	10.06	3.67	2.33	0.66	98.05	41.93
	VS-73	45.80	3.33	14.82	11.10	0.03	0.12	4.53	9.98	3.68	2.13	0.47	95.99	42.08
	VS-74	46.54	3.59	15.91	11.31	–	0.17	4.49	10.25	3.89	2.14	0.44	98.73	41.44
SW8	VS-75	47.49	3.52	14.64	10.67	0.00	0.15	4.64	10.34	3.52	2.18	0.58	97.73	43.69
	VS-76	47.66	3.72	14.39	10.78	0.03	0.15	4.68	10.41	3.81	2.25	0.63	98.50	43.66
	VS-77	47.64	3.47	14.81	10.72	0.02	0.11	4.71	10.49	3.75	2.27	0.69	98.65	43.94
	VS-78	47.12	3.53	14.64	10.61	–	0.23	4.65	10.34	3.66	2.25	0.65	97.67	43.86
	VS-79	47.86	4.23	14.65	11.27	–	0.23	4.03	9.36	3.87	2.48	0.77	98.75	38.91
	VS-80	47.71	3.28	14.85	11.14	0.02	0.18	4.27	10.32	3.62	2.40	0.58	98.36	40.58
	VS-81	49.76	2.89	15.30	9.44	–	0.12	4.32	9.64	3.38	2.45	0.71	97.99	44.90
	VS-82	47.35	3.38	14.50	10.89	0.03	0.18	4.53	10.32	3.49	2.29	0.70	97.65	42.57
	VS-83	48.09	3.75	14.62	12.30	–	0.17	3.60	8.86	3.65	2.84	0.71	98.60	34.30
	VS-84	47.55	3.24	14.79	10.90	–	0.20	4.66	10.16	3.65	2.28	0.66	98.07	43.26
	VS-85	47.81	3.65	14.59	12.99	0.01	0.17	3.49	8.15	3.66	3.08	0.65	98.25	32.38
	VS-86	50.13	3.02	15.52	9.41	–	0.16	3.86	8.86	3.99	2.51	–	97.44	42.20
	VS-87	46.97	3.49	14.71	10.98	0.02	0.11	4.55	10.05	3.88	2.24	–	97.00	42.50
	VS-88	49.87	2.56	16.19	9.24	–	0.15	4.01	7.63	4.29	2.78	–	96.71	43.60
	VS-89	47.03	3.58	14.75	11.10	0.05	0.17	4.55	9.98	3.90	2.26	–	97.36	42.24
	VS-90	47.76	3.33	14.78	10.85	–	0.15	4.51	9.96	3.95	2.32	–	97.60	42.54
	VS-91	47.33	3.54	14.75	11.19	0.07	0.21	4.60	10.02	3.62	2.18	0.92	98.42	42.29

**Table 1.** (continued)

Sample no.	ID	SiO <sub>2</sub>	TiO <sub>2</sub>	Al <sub>2</sub> O <sub>3</sub>	FeO*	Cr <sub>2</sub> O <sub>3</sub>	MnO	MgO	CaO	Na <sub>2</sub> O	K <sub>2</sub> O	P <sub>2</sub> O <sub>5</sub>	Total	Mg#
SW9	VS-92	47.11	3.52	14.31	11.38	0.02	0.22	4.75	10.19	3.71	2.28	0.59	98.07	42.64
	VS-93	48.16	3.88	14.41	11.53	0.05	0.16	4.01	9.18	3.84	2.58	0.70	98.48	38.24
	VS-94	47.64	3.52	15.08	10.98	0.09	0.20	4.56	10.50	3.60	2.13	0.57	98.87	42.52
	VS-95	46.49	3.30	14.28	10.33	0.04	0.12	4.62	10.27	3.73	2.14	0.61	95.91	44.36
	VS-96	47.81	3.30	14.64	10.97	—	0.18	4.53	10.04	3.68	2.27	0.63	98.03	42.42
	VS-97	48.04	3.00	14.65	11.23	0.02	0.22	4.52	10.33	3.76	2.28	0.62	98.67	41.74
	VS-98	47.63	3.44	14.61	11.05	0.03	0.15	4.71	10.27	3.73	2.25	0.67	98.54	43.15
	VS-99	47.84	3.66	14.52	11.52	—	0.19	4.13	9.63	3.83	2.52	0.71	98.54	38.99
SW10	VS-100	48.20	3.37	14.50	11.08	—	0.18	4.46	10.37	3.33	2.04	0.59	98.12	41.74
SW11	VS-101	47.74	3.18	15.14	10.54	0.04	0.18	4.63	10.62	3.78	2.00	0.57	98.42	43.90
	VS-102	47.10	3.81	14.68	10.91	0.04	0.14	4.25	9.29	3.87	2.32	0.63	97.04	40.99
	VS-103	47.32	3.50	14.65	10.90	0.00	0.20	4.49	10.21	3.67	2.11	0.63	97.68	42.35
	VS-104	47.85	3.64	14.63	11.42	—	0.17	4.20	9.83	3.85	2.19	0.70	98.48	39.59
	VS-105	47.25	3.81	14.59	10.55	—	0.20	4.44	10.25	3.78	2.08	0.59	97.54	42.86
	VS-106	47.53	3.61	14.66	11.19	—	0.15	4.51	10.24	3.38	2.12	0.60	98.00	41.81
SW12	VS-107	47.46	3.22	14.59	10.67	—	0.17	4.71	10.58	3.54	1.99	0.61	97.53	44.03
	VS-108	47.13	3.12	14.60	10.66	0.04	0.15	4.75	10.51	3.70	2.02	0.58	97.26	44.26
	VS-109	47.59	3.36	14.76	10.89	—	0.17	4.76	10.44	3.80	2.03	0.65	98.45	43.77
	VS-110	47.50	3.31	14.50	10.77	—	0.17	4.64	10.42	3.67	2.03	0.57	97.58	43.41
	VS-111	47.34	3.35	14.67	10.89	—	0.15	4.72	10.55	3.65	2.06	0.74	98.11	43.60
	VS-112	47.58	3.22	14.55	10.73	0.05	0.17	4.69	10.18	3.81	2.22	0.55	97.73	43.8
	VS-113	47.44	3.45	14.44	10.95	—	0.18	4.71	10.15	3.62	2.23	0.69	97.84	43.4
	VS-114	47.56	3.32	14.38	10.65	0.06	0.24	4.56	10.31	3.60	2.11	0.67	97.47	43.3
	VS-115	47.38	3.57	14.58	10.74	—	0.17	4.80	10.47	3.73	2.03	0.64	98.11	44.3
	VS-116	47.13	3.23	14.71	11.15	—	0.25	4.45	9.85	3.75	2.31	1.08	97.91	41.6
	VS-117	47.60	3.42	14.76	10.94	0.01	0.17	4.71	10.22	3.67	2.17	—	97.68	43.4
	VS-118	47.18	3.23	14.60	11.03	0.00	0.10	4.54	10.27	3.78	2.20	—	96.93	42.3
	VS-119	47.19	3.55	14.53	10.99	0.02	0.17	4.45	10.07	3.66	2.26	0.92	97.79	41.9
	VS-120	46.99	3.39	14.46	11.46	0.03	0.19	4.55	9.83	3.72	2.29	—	96.92	41.4
SW13	VS-121	47.87	3.56	14.57	10.94	—	0.17	4.70	10.19	3.64	2.05	0.54	98.21	43.4
	VS-122	47.71	3.37	14.92	10.98	—	0.18	4.65	10.30	3.74	2.12	0.60	98.56	43.0
	VS-123	47.14	3.49	14.65	11.05	—	0.19	4.45	10.34	3.70	2.05	0.71	97.77	41.8
SW14	VS-124	47.27	3.57	14.69	10.72	0.03	0.12	4.73	10.46	3.78	2.07	0.58	98.00	44.0
	VS-125	47.09	3.31	14.76	11.12	0.01	0.24	4.47	10.30	3.75	2.07	0.59	97.69	41.7
	VS-126	47.26	3.47	14.70	10.67	—	0.18	4.65	10.34	3.67	1.98	0.67	97.58	43.7
	VS-127	47.18	3.18	14.70	10.25	0.02	0.13	5.02	10.50	3.81	2.03	0.58	97.41	46.6
	VS-128	47.70	3.27	14.77	10.73	—	0.18	4.66	10.56	3.64	2.04	0.63	98.19	43.6
	VS-129	50.93	2.06	16.64	8.66	0.04	0.13	4.07	7.88	4.29	2.69	—	97.38	45.6
	VS-130	49.38	2.81	15.20	9.70	—	0.19	4.50	9.53	3.60	2.39	0.77	98.06	45.2
	VS-131	47.04	2.98	14.92	10.72	0.06	0.17	5.04	10.56	3.56	2.04	—	97.09	45.6
	VS-132	47.98	3.22	14.96	10.41	—	0.23	5.00	10.98	3.38	2.00	—	98.15	46.1
	VS-133	50.77	2.28	16.76	8.59	0.02	0.14	3.94	7.74	4.31	2.88	0.16	97.60	45.0
	VS-134	50.82	2.31	16.21	8.68	—	0.12	4.76	8.00	4.19	2.58	0.16	97.81	49.4
SW15	VS-135	47.91	3.42	14.70	11.01	0.05	0.14	4.74	10.45	3.76	2.12	0.54	98.83	43.4
	VS-136	47.52	3.29	14.71	10.04	0.04	0.23	4.82	10.62	3.60	2.05	0.58	97.48	46.1
	VS-137	47.84	3.15	14.72	10.14	0.09	0.21	4.93	10.50	3.55	2.03	0.53	97.69	46.4
	VS-138	47.96	3.28	14.98	10.21	0.03	0.20	5.01	10.85	3.44	1.95	0.46	98.37	46.7

**Table 1.** (continued)

Sample no.	ID	SiO <sub>2</sub>	TiO <sub>2</sub>	Al <sub>2</sub> O <sub>3</sub>	FeO*	Cr <sub>2</sub> O <sub>3</sub>	MnO	MgO	CaO	Na <sub>2</sub> O	K <sub>2</sub> O	P <sub>2</sub> O <sub>5</sub>	Total	Mg#
SW16	VS-139	47.42	3.31	14.82	10.25	0.03	0.19	5.13	10.67	3.41	1.87	0.58	97.66	47.1
	VS-140	47.48	2.93	14.43	10.17	0.04	0.15	5.10	10.57	3.48	1.92	0.49	96.75	47.2
	VS-141	47.24	3.93	14.74	10.83	0.00	0.15	4.11	9.44	3.64	2.16	0.76	97.00	40.3
	VS-142	48.22	3.04	14.72	10.50	–	0.13	5.05	10.84	3.27	2.04	0.53	98.32	46.1
	VS-143	47.16	3.07	14.35	10.35	0.01	0.18	5.21	10.40	3.62	2.07	0.53	96.92	47.3
SW17	VS-144	47.81	2.92	14.75	10.58	0.02	0.15	4.99	10.73	3.39	1.95	0.50	97.79	45.7
	VS-145	47.65	2.98	14.67	10.16	0.01	0.23	5.25	10.83	3.46	1.86	0.54	97.63	47.9
	VS-146	47.83	2.93	15.09	10.26	–	0.11	5.25	10.81	3.44	1.88	0.57	98.16	47.7
	VS-147	48.04	3.02	14.76	10.17	0.04	0.15	5.05	10.70	3.45	1.81	0.56	97.76	46.9
	VS-148	47.20	3.29	14.43	10.48	0.03	0.11	5.07	10.67	3.49	1.88	0.52	97.16	46.3
	VS-149	47.86	3.08	14.92	10.16	0.02	0.11	5.19	10.84	3.60	1.93	0.58	98.30	47.7
	VS-150	47.58	3.32	14.66	10.87	–	0.17	4.35	10.10	3.84	2.19	2.14	99.22	41.7
	VS-151	49.20	2.46	15.77	9.52	–	0.14	4.72	8.73	3.89	2.58	0.16	97.16	46.9
	VS-152	47.49	3.21	14.89	11.01	0.06	0.19	4.44	10.21	3.63	2.25	–	97.37	41.8
	VS-153	49.46	2.65	15.56	9.17	0.02	0.14	5.03	9.12	3.83	2.40	0.46	97.84	49.4
SW18	VS-154	50.82	2.30	16.82	8.73	–	0.13	3.88	7.30	4.38	3.04	1.09	98.50	44.2
	VS-155	48.49	2.65	15.54	10.09	0.04	0.14	4.99	8.62	3.92	2.50	1.08	98.04	46.9
	VS-156	51.52	2.03	16.79	8.40	0.01	0.11	3.71	7.63	4.11	2.72	0.79	97.84	44.1
	VS-157	47.72	2.97	14.88	10.18	–	0.17	5.12	10.81	3.45	1.92	0.48	97.69	47.3
	VS-158	47.53	3.02	14.62	10.00	0.06	0.19	5.12	10.81	3.51	1.84	0.53	97.24	47.7
	VS-159	47.40	3.08	14.95	9.94	0.05	0.19	5.15	10.70	3.56	1.89	0.58	97.46	48.0
SW18	VS-160	48.26	3.30	14.73	10.22	0.03	0.19	5.26	10.67	3.36	1.94	0.59	98.53	47.9
	VS-161	47.77	3.27	14.84	10.35	0.03	0.17	5.15	10.72	3.33	1.92	0.54	98.09	47.0
	VS-162	47.82	2.72	14.83	10.20	–	0.12	5.26	10.68	3.41	1.84	0.51	97.38	47.9
	VS-163	48.04	2.84	15.01	10.44	0.03	0.16	4.98	10.89	3.43	1.91	0.54	98.25	45.9
	VS-164	47.90	3.02	14.99	10.33	0.02	0.14	5.01	10.94	3.48	1.94	0.54	98.31	46.4

Note: FeO\* = Total Fe as FeO\*, Mg# =  $100Mg^{2+}/(Mg^{2+} + Fe^{2+})$ , VS = vesicular sideromelane grain.

block-sized, non-vesicular and angular glassy particles that are interpreted to be hyaloclastite or pillow fragment breccia. This layer is 24 m thick (core depth: 48–72 m) and is underlain by the Seoguipo Formation. The Seoguipo Formation is 73 m thick (core depth: 72–145 m) and is composed of well-sorted, coarse-to fine-grained, shell-rich volcaniclastic sand with intercalated sandy mudstones. The U Formation beneath the Seoguipo Formation occurs at a core depth of > 145 m and is composed of unconsolidated quartzose sand and mud. The basement was not found at this site because the core did not reach the basement. Therefore, the thickness of the U Formation and the lithofacies of the basement could not be identified. However, the lithology of the basement could be inferred to be the quartzose metasedimentary rocks based on the accidental clasts in the tuff beds of Suwolbong.

Based on the lithology of the subsurface strata, the origin of the accidental particles could be classified as follows:

1) Crystalline basalt fragments consisting of abundant olivine and plagioclase phenocrysts in a microcrystalline groundmass rich in plagioclase laths are interpreted to have been derived from the underlying lavas (Fig. 9b).

2) Basaltic glasses derived from the volcaniclastic units of the Seoguipo Formation formed by phreatomagmatic eruptions are difficult to distinguish from juvenile glass when present as solitary particles. To distinguish between them, we examined the microscopic texture of the accidental tuff blocks from the Seoguipo Formation within the Suwolbong tuff ring. The vesicular basalt glasses of the Seoguipo Formation were identified to be characterized by palagonite rims or secondary minerals along the particle margins and in the vesicle walls (e.g., Go et al., 2017). Vesicular basaltic glasses with these characteristics are interpreted to have been derived from the Seoguipo Formation (Fig. 9c).

3) In the thin sections of the tuff blocks of the Seoguipo Formation, non-vesicular glasses were also found with alteration rims and subalkaline composition (Fig. 9d). The non-vesicular glass in the tuff blocks of the Seoguipo Formation has a total alkali content of 3.7–3.9 wt% and a SiO<sub>2</sub> content of 52.7–54.1 wt%, which corresponds to the subalkaline series of basaltic andesite. They are plotted in the same assemblages as those of the Suwolbong tuff ring on a TAS diagram (Table 2, Fig. 6a). These glasses show mingling texture between the subalkaline and alkaline glass, which

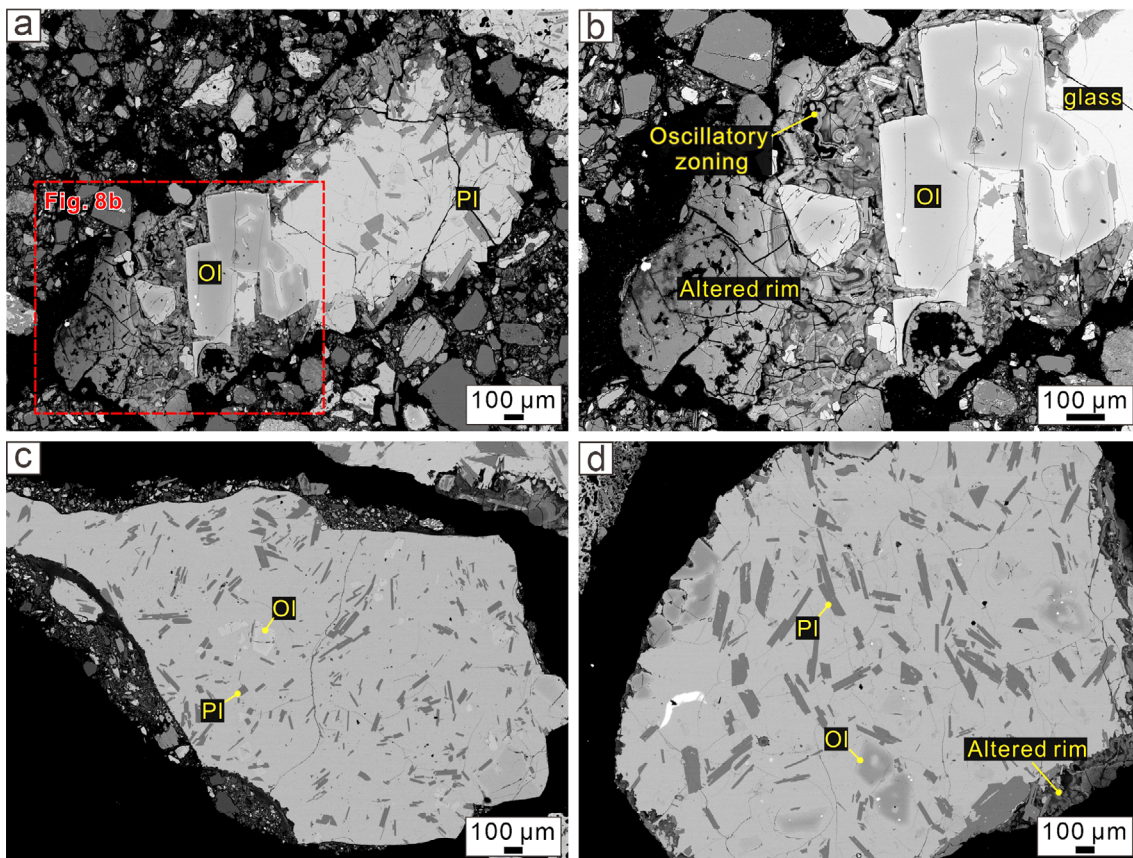


**Fig. 8.** Back-scattered electron (BSE) images of non-vesicular glass of alkaline to subalkaline composition (a, b) Non-vesicular grains having altered or palagonitized rims along grain margins and vesicle walls. (c, d) Subtypes of non-vesicular glass based on crystal size and geochemical composition. Ol: olivine and Pl: plagioclase.

indicates the mixing of the alkaline and subalkaline magma (Fig. 9e). The features of the non-vesicular glasses are consistent with the texture of the hyaloclastite in cores throughout the Jeju Island (Jeong and Sohn, 2011; Koh et al., 2019, 2020; Jeon et al., 2022). The non-vesicular glasses are inferred to be hyaloclastite fragments derived from either the intercalated layers of the Seoguipo Formation or at the bottom of the lava unit, not juvenile materials (see the discussion for more details).

4) Monocrystalline quartz grains have angular to subrounded shapes and internal fractures. They are contained within basaltic tuff fragments or occur in aggregates consisting of particles of various sizes with a clayey matrix. Most of these particles are interpreted as being derived from the U Formation, with some derived from the Seoguipo Formation (Fig. 9f).

5) Polycrystalline quartz grains with internal fractures and several micropores. These grains were interpreted as derived from quartzose metasedimentary rocks of unknown ages (Go et al., 2017).

6) Accessory mineral grains of alkali feldspar and heavy minerals are also interpreted to have been derived from the basement rocks (Fig. 9g).

## 6. DISCUSSION

### 6.1. Recognition of Juvenile and Accidental Glassy Pyroclasts

Based on the microscopic observations and geochemical analysis of the entire tuff sequence of Suwolbong, we interpret that only vesicular glassy pyroclasts with an alkali composition, mainly containing olivine, clinopyroxene, and plagioclase, are juvenile, as explained below.

(1) Vesicular glassy pyroclasts show a correlation between the vesicularity change and the lithofacies change in the outcrop. The average vesicularity of these pyroclasts, calculated from the cross-sectional area of the vesicles, ranges between 4 and 15%, with an overall decreasing trend in ascending stratigraphic order, with two peaks corresponding to the breccia layers in the outcrop (Fig. 5). The upward-decreasing vesicularity indicates rapid ascent of magma supplied by magma pulses, followed by a gradual decrease in magma flux and degassing during eruption (Houghton and Wilson, 1989; Bamber et al., 2024). In contrast, non-vesicular pyroclasts do not show any systematic variation in vesicularity

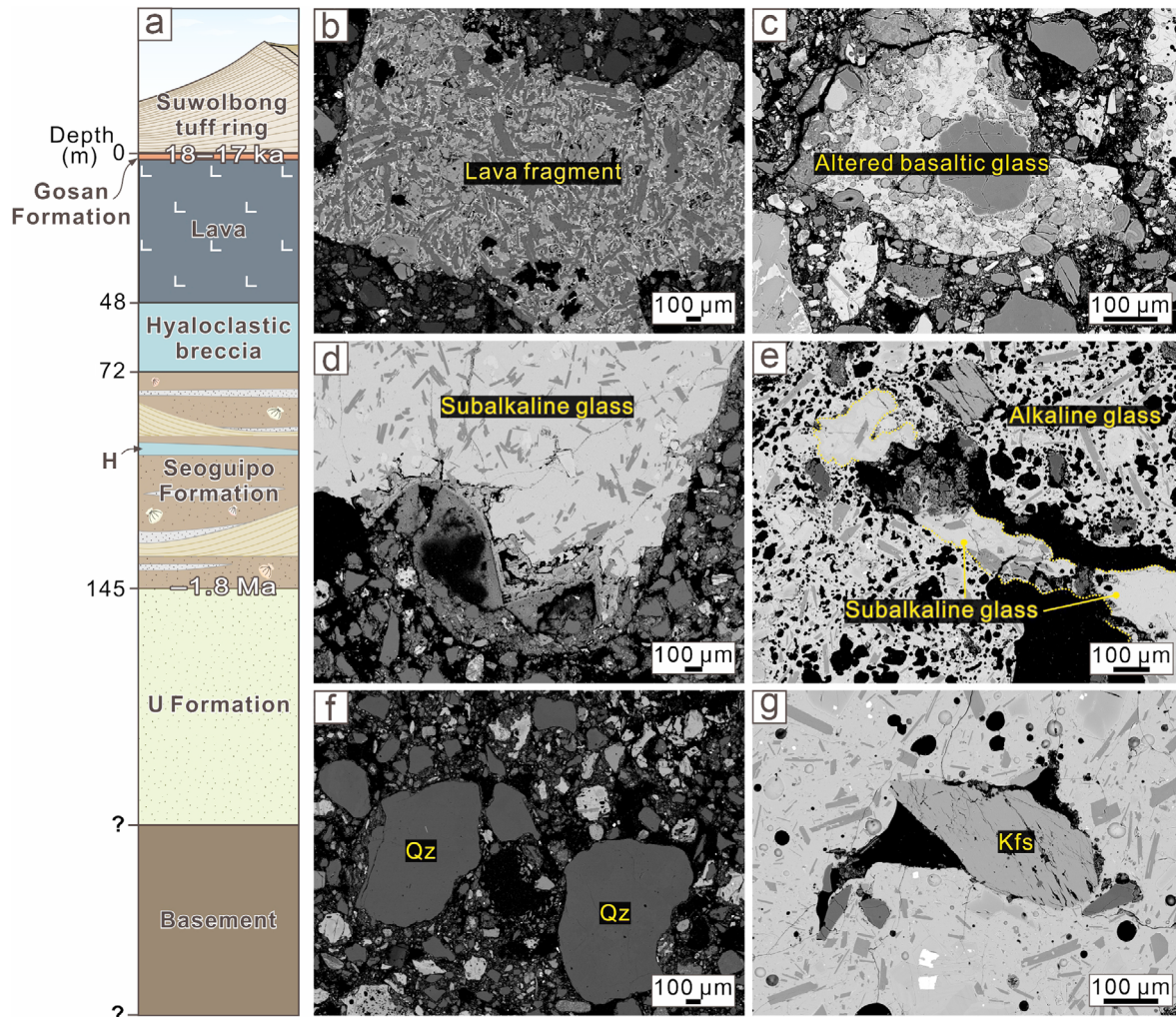


**Fig. 9.** Susurface stratigraphy of the Suwolbong tuff ring and back-scattered electron (BSE) images of accidental materials. (a) Sedimentary log as inferred from borehole data. (b) Crystalline basalt fragments derived from the underlying lavas. (c) Altered basaltic glass with alkaline composition derived from the Seoguipo Formation. (d, e) Non-vesicular glass with subalkaline composition in the tuff block derived from the Seoguipo Formation. (f) Monocrystalline quartz grains derived mainly from the U Formation. (g) Accessory mineral grains derived from the basement. H: hyaloclastite.

or crystallization, and the very low vesicularity (0–5%) and some large vesicles indicate that the particles were fragmented from already degassed magma or lava (Polacci et al., 2008; Okumura et al., 2009). The differences in vesicularities and crystallization patterns of the two pyroclasts indicate that they were formed through different processes, although they were ejected from the same crater and deposited together. Hence, it is reasonable to interpret that one of the pyroclasts, i.e., the non-vesicular glass, originated from the substrate.

(2) The non-vesicular subalkaline basaltic glass has an alteration rim. Most of the surrounding vesicular pyroclasts in the same layer are fresh and unaltered. Volcanic glass is not likely to be selectively altered grain by grain. All basaltic glass in the same deposits is likely to be altered all together (Geshi et al., 2011; Valentine and Connor, 2015). Therefore, the non-vesicular glass is interpreted to have formed prior to the eruption of the Suwolbong

tuff ring, being subject to diverse alteration processes before excavation by explosive eruptions of the Suwolbong.

(3) Hyaloclastites with subalkaline compositions are intercalated in the Seoguipo Formation and beneath the lava substrate. The characteristics of the hyaloclastite, confirmed through borehole data and microscopic observations of accidental rock fragments, are similar to those of non-vesicular glass observed in the Suwolbong tuff ring (Koh et al., 2019; Jeon et al., 2022). An optical televiewer (OPTV) image of the hyaloclastite layer in a borehole in the eastern part of Jeju Island shows that the interstices between volcaniclastic rocks of various sizes are filled with a brown to light brown matrix that has undergone palagonization (Koh et al., 2019). These characteristics are consistent with those typical of hyaloclastite (Cas and Wright, 1987; McPhie et al., 1993) and correspond well to those of the non-vesicular glass found in the Suwolbong tuff ring. SEM-BSE imaging of a thin section of

**Table 2.** Major element composition of glassy groundmass of accidental grains in the Suwolbong tuff samples

Sample no.	ID	SiO <sub>2</sub>	TiO <sub>2</sub>	Al <sub>2</sub> O <sub>3</sub>	FeO*	Cr <sub>2</sub> O <sub>3</sub>	MnO	MgO	CaO	Na <sub>2</sub> O	K <sub>2</sub> O	P <sub>2</sub> O <sub>5</sub>	Total
SW1	NVS-1	53.81	2.30	13.74	10.31	0.04	0.16	5.12	8.76	3.28	0.59	0.21	98.31
	NVS-2	49.79	3.21	14.31	10.33	0.03	0.17	4.96	10.03	3.46	1.81	0.54	98.63
SW2	NVS-3	53.63	2.37	13.91	10.48	–	0.11	5.13	8.89	3.24	0.66	0.22	98.64
	NVS-4	53.23	2.06	13.90	10.38	0.02	0.13	5.31	8.69	3.19	0.60	0.21	97.71
SW3	NVS-5	54.38	2.00	14.03	10.39	0.03	0.11	5.03	8.88	3.18	0.61	0.15	98.79
	NVS-6	48.98	3.56	12.50	12.15	0.02	0.25	5.54	10.11	3.41	1.79	0.65	98.94
	NVS-7	49.33	3.01	14.36	10.57	0.03	0.20	5.06	10.13	3.35	1.81	0.58	98.44
SW4	NVS-8	49.26	3.22	14.14	10.83	–	0.14	4.98	10.02	3.63	1.88	0.56	98.65
	NVS-9	49.39	3.20	14.02	10.62	–	0.16	5.03	9.94	3.40	1.84	0.64	98.26
SW5	NVS-10	49.47	3.18	14.08	10.10	0.03	0.14	5.10	10.07	3.51	1.78	0.56	98.01
	NVS-11	49.12	3.18	14.50	10.31	0.06	0.15	5.08	10.10	3.46	1.94	0.64	98.53
	NVS-12	49.38	3.09	14.23	10.35	0.01	0.13	5.03	9.98	3.54	1.81	0.59	98.13
	NVS-13	49.76	3.23	14.27	10.42	0.02	0.18	4.80	10.02	3.68	1.79	0.53	98.69
	NVS-14	49.31	3.16	14.12	10.18	0.06	0.15	4.83	9.93	3.51	1.77	0.56	97.58
	NVS-15	54.26	2.36	13.75	10.83	0.03	0.15	5.11	8.85	3.16	0.62	0.25	99.38
	NVS-16	49.52	3.27	14.13	10.38	0.04	0.15	4.96	10.11	3.51	1.83	0.52	98.41
	NVS-17	49.49	3.02	14.32	9.37	0.05	0.18	4.97	9.97	3.50	1.81	0.58	97.26
SW6	NVS-18	49.29	3.01	14.17	11.06	0.10	0.19	5.08	9.69	3.58	1.87	0.47	98.50
	NVS-19	54.34	2.42	13.91	10.11	0.06	0.18	5.13	8.81	3.15	0.60	0.20	98.91
	NVS-20	54.20	2.37	13.89	10.68	0.04	0.18	4.99	8.75	3.10	0.60	0.22	99.03
	NVS-21	54.02	2.11	13.72	10.19	0.05	0.15	5.26	8.73	3.25	0.60	0.28	98.36
	NVS-22	53.98	1.98	14.01	10.67	–	0.14	5.44	8.92	3.13	0.60	0.15	99.01
	NVS-23	48.50	3.23	14.13	10.57	–	0.17	4.92	10.29	3.57	1.87	0.53	97.77
SW9	NVS-24	49.02	3.34	14.40	10.66	0.02	0.17	4.91	10.27	3.60	1.85	0.61	98.85
	NVS-25	50.51	3.58	13.44	11.30	0.01	0.17	4.70	9.24	3.70	1.53	0.51	98.68
	NVS-26	53.89	2.30	14.15	10.50	0.09	0.15	5.24	8.85	3.31	0.61	0.20	99.29
	NVS-27	54.33	2.11	13.95	10.23	0.03	0.14	5.14	8.72	3.23	0.61	0.21	98.69
	NVS-28	54.28	2.17	14.23	10.44	0.03	0.15	5.30	8.68	3.24	0.61	0.21	99.34
	NVS-29	49.68	3.33	14.36	10.19	–	0.13	5.08	10.20	3.62	1.82	0.59	98.99
SW10	NVS-30	53.47	2.30	13.64	10.42	0.08	0.18	5.04	8.80	3.28	0.61	0.26	98.07
	NVS-31	48.93	2.97	14.32	10.49	0.04	0.15	5.12	10.24	3.47	1.68	0.65	98.06
SW11	NVS-32	48.74	3.33	14.28	10.58	0.01	0.20	5.22	10.32	3.53	1.69	0.59	98.47
	NVS-33	53.83	2.20	13.85	10.61	0.06	0.09	5.13	8.80	3.26	0.59	0.18	98.58
	NVS-34	50.73	3.11	13.28	11.27	–	0.14	4.81	9.19	3.39	1.46	0.58	97.96
	NVS-35	53.62	2.22	13.55	10.80	–	0.22	5.29	8.79	3.16	0.56	0.25	98.45
	NVS-36	54.02	2.42	13.38	10.77	0.04	0.15	5.18	8.85	3.20	0.59	0.20	98.81
	NVS-37	53.66	2.38	13.74	10.53	0.10	0.11	5.04	8.76	3.21	0.55	0.19	98.26
SW12	NVS-38	50.49	3.37	13.72	10.88	0.02	0.24	4.78	9.29	3.29	1.36	0.61	98.03
	NVS-39	51.48	3.57	13.20	11.91	–	0.14	4.54	8.79	2.94	1.56	0.61	98.74
	NVS-40	53.83	2.21	13.47	10.51	0.05	0.15	5.04	8.68	3.35	0.56	0.20	98.04
SW13	NVS-41	49.09	3.27	14.42	10.59	–	0.13	5.14	10.16	3.59	1.62	0.51	98.50

**Table 2.** (continued)

Sample no.	ID	SiO <sub>2</sub>	TiO <sub>2</sub>	Al <sub>2</sub> O <sub>3</sub>	FeO*	Cr <sub>2</sub> O <sub>3</sub>	MnO	MgO	CaO	Na <sub>2</sub> O	K <sub>2</sub> O	P <sub>2</sub> O <sub>5</sub>	Total
SW14	NVS-42	53.50	2.28	13.91	10.36	0.04	0.08	5.27	8.79	3.36	0.54	0.20	98.33
	NVS-43	53.81	1.85	13.96	10.17	0.02	0.15	5.26	7.87	3.13	0.50	0.19	96.91
	NVS-44	53.57	2.25	14.05	10.33	0.03	0.16	5.16	8.76	3.28	0.58	0.22	98.39
	NVS-45	53.35	2.05	13.90	9.99	0.03	0.14	5.12	8.85	3.21	0.57	0.22	97.43
	NVS-46	53.62	2.17	13.73	10.08	–	0.14	5.19	8.93	3.27	0.50	0.26	97.88
	NVS-47	53.85	2.23	13.55	10.31	0.08	0.14	5.33	8.88	3.18	0.56	0.19	98.29
	NVS-48	53.50	2.04	14.00	10.54	0.04	0.11	5.30	8.73	3.25	0.56	0.22	98.30
SW16	NVS-49	51.09	2.99	13.69	11.15	–	0.21	4.54	9.04	3.28	1.46	0.63	98.07
SW17	NVS-50	50.12	3.14	13.39	10.20	0.05	0.16	4.79	9.19	3.39	1.35	0.61	96.40
	NVS-51	50.59	3.09	13.38	10.93	0.02	0.21	4.78	9.32	3.24	1.39	0.63	97.58
SW18	NVS-52	51.82	3.29	13.43	11.02	–	0.13	4.48	8.85	2.91	1.52	0.44	97.89
	NVS-53	55.32	2.19	13.53	11.07	0.04	0.17	5.00	8.92	2.10	0.58	0.32	99.24
SF	SF-1	53.79	2.52	13.69	10.82	–	0.15	5.01	8.61	3.27	0.59	0.23	98.67
	SF-2	47.07	3.94	14.46	11.90	–	0.18	4.21	9.36	3.84	2.39	0.64	97.99
	SF-3	53.52	2.32	13.52	11.27	0.01	0.12	4.86	8.66	3.21	0.63	0.18	98.29
	SF-4	54.10	2.37	13.63	10.86	0.01	0.13	4.98	8.62	3.10	0.62	0.22	98.63
	SF-5	51.02	2.73	15.91	9.34	0.01	0.14	3.66	7.64	3.88	2.85	0.59	97.77
	SF-6	49.14	3.36	14.35	11.02	0.01	0.14	4.97	9.94	3.74	1.85	0.51	99.03
	SF-7	50.13	2.45	16.63	9.28	0.03	0.14	4.28	8.14	3.92	2.62	0.53	98.15
	SF-8	49.72	2.94	16.16	9.73	0.02	0.20	3.60	7.59	4.24	2.86	0.86	97.92
	SF-9	50.44	2.84	16.33	9.30	0.03	0.14	3.83	7.57	4.42	2.85	0.74	98.49
	SF-10	50.27	2.68	16.06	8.85	0.02	0.13	4.54	8.27	4.16	2.43	0.50	97.90
	SF-11	49.39	2.80	16.27	9.19	–	0.14	3.77	7.61	4.29	2.78	0.56	96.80
	SF-12	49.66	2.99	15.98	9.73	–	0.14	3.86	7.85	4.19	2.83	0.61	97.86
	SF-13	49.52	3.10	15.76	9.87	–	0.11	3.69	7.55	4.11	3.00	0.68	97.38
	SF-14	50.42	3.08	15.05	10.25	–	0.18	3.23	7.48	4.30	3.50	0.75	98.24
	SF-15	46.39	3.93	14.89	11.91	–	0.18	3.89	9.30	4.02	2.44	0.60	97.56
	SF-16	47.08	3.92	14.96	11.51	0.03	0.17	4.14	9.34	4.08	2.51	0.56	98.29
	SF-17	48.62	3.25	15.97	10.63	–	0.17	3.95	8.53	4.05	2.60	0.68	98.45
	SF-18	47.85	3.45	14.65	11.43	–	0.17	4.01	9.11	3.61	2.59	0.51	97.36
	SF-19	46.64	3.60	14.63	11.80	0.03	0.20	4.12	9.41	3.90	2.34	0.51	97.17
	SF-20	46.55	3.96	15.06	11.52	–	0.16	4.22	9.50	3.90	2.33	0.61	97.79
	SF-21	46.56	3.33	15.19	11.89	–	0.12	4.09	9.14	3.49	2.27	0.61	96.69
	SF-22	52.71	2.29	13.53	10.91	0.07	0.13	5.06	8.60	3.27	0.61	0.19	97.38
	SF-23	49.10	3.07	15.18	9.72	–	0.18	4.11	9.07	3.82	2.33	0.66	97.22
	SF-24	46.82	3.98	14.79	11.65	0.01	0.25	4.05	9.33	4.09	2.30	0.47	97.72
	SF-25	48.97	2.52	15.45	9.53	0.06	0.14	4.90	9.91	3.68	2.08	0.41	97.64

Note: FeO\* = Total Fe as FeO\*, NVS = Non-vesicular sideromelane grain, SF = Seoguipo Formation.

hyaloclastite showing non-vesicular alteration rims of hemispherical oscillatory zoning from the northeastern core data reported on Jeju Island is also consistent with the textural characteristics of the non-vesicular glass of the Suwolbong tuff ring (Jeong and Sohn, 2011). These features suggest that the non-vesicular glass is not a juvenile product of phreatomagmatic eruptions but rather an accidental material derived from the hyaloclastite layers that were deposited before the eruption of the Suwolbong tuff ring.

The presence of hyaloclastites serves as an indicator of paleosea-

levels, providing a clue to surface environment at the time of formation (Koh et al., 2015; Smellie and Edwards, 2016). In Jeju Island, hyaloclastite is present below sea level in low-altitude areas except in the southern part of the island (Koh et al., 2015). In the west, where the Suwolbong tuff ring is located, the hyaloclastite is divided into two age groups, 320–220 ka and 160–110 ka, based on <sup>40</sup>Ar-<sup>39</sup>Ar ages of borehole samples (Koh et al., 2015). The subdivision of the non-vesicular glass into two group in the Suwolbong tuff, based on microtexture and chemical properties,

indicates the presence of more than two layers of chemically different hyaloclastite in the subsurface. Thus, it is clear that it has undergone several environmental changes due to sea-level fluctuations before the formation of the Suwolbong tuff ring, although the formation age of the hyaloclastite in the lower part of the volcano cannot be precisely determined. It has been reported that the sea level was  $-120$  to  $-130$  m lower than today during 18–17 ka when the Suwolbong tuff ring formed and that the volcano erupted in a subaerial environment (Cheong et al., 2007). These conditions also suggest that hyaloclastites did not form during the eruption of Suwolbong.

## 6.2. Magma Plumbing System of the Suwolbong Tuff Ring

The characteristics of the newly defined juvenile pyroclasts of Suwolbong suggest that the tuff ring was formed from alkaline magmas ascending through a rather simple magma-plumbing system. Additionally, analysis of the anisotropy of magnetic susceptibility (AMS) of pyroclastic deposits of the Suwolbong tuff ring suggests that the tephra originated from a single source vent (Cho et al., 2021). Therefore, The magma plumbing system of the Suwolbong tuff ring is inferred to have been sourced by at least three magma batches independently ascending and erupting

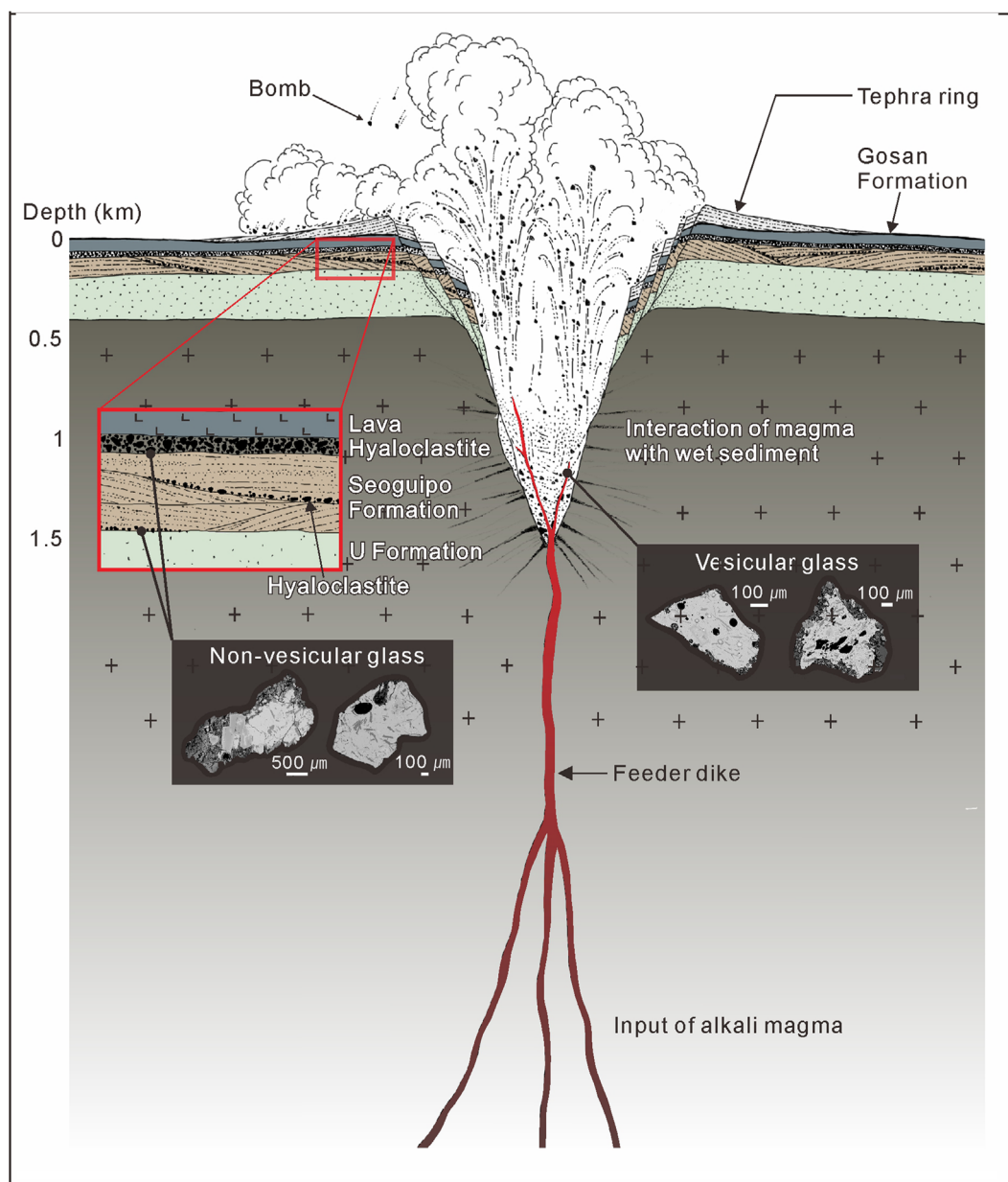


**Fig. 10.** Schematics of the magma plumbing system during the eruption at Suwolbong. The Suwolbong plumbing system was sourced by at least three independent magma batches that ascended and erupted in sequence from a single large dike system without magma mixing. Vesicular glass resulted from the fragmentation of injected fresh magma, while non-vesicular glass originated from multiple subsurface hyaloclastite layers.

from the same crater without interaction between them during the magma ascent (Fig. 10).

A previous study suggested that the Suwolbong tuff ring was formed from alkaline to subalkaline magmas that ascended through a complex, congested magma-plumbing system (Brenna et al., 2011). Brenna et al. (2011) also suggested that the pyroclasts of Suwolbong had partially mixed compositions, intermediate between the two end-member magmas of Udo, which is one of the monogenetic volcanoes on Jeju Island, suggesting that there were interactions and mixing between magmas from different sources (Fig. 4). However, our results show that the pyroclasts of the intermediate composition, i.e., the non-vesicular glasses are accidental. Juvenile vesicular pyroclasts are found to be only alkaline in composition. The stepped and oscillating chemical trend of Suwolbong reported in the previous study (Brenna et al., 2011, Fig. 4b) is therefore thought to be the result of analysis without distinguishing between juvenile and accidental particles. A simpler chemical trend is observed when the accidental subalkali components are excluded. This suggests that the magma plumbing system of Suwolbong resulted from an initial magma pulse followed by several independently ascending and evolving magma pulses without interactions between them (Smith and Nemeth, 2017). The stepped and oscillating chemical trend of Brenna et al. (2011) is more likely related to the substrate excavation and material mixing processes within the subsurface diatreme of the Suwolbong tuff ring. Accidental materials, such as sub-alkaline hyaloclastite fragments and detrital quartz grains, are interpreted to have been excavated from subsurface strata, hundreds of meters deep, and then deposited on the surface together with juvenile particles, resulting in a wide range of compositions of pyroclasts in the same depositional units.

Another cause of errors in chemical analysis of pyroclasts is the presence of many non-volcanic accidental materials, such as detrital quartz grains and heavy minerals, in the alkali glass. These accidental materials inevitably lead to errors in chemical analysis results when the analysis is made by whole-rock analysis.

Polymagmatic activity, in which alkaline and subalkaline magmas are produced together, has been reported in Udo, one of the monogenetic volcanoes on Jeju Island (Brenna et al., 2010). The volcano differs from the Suwolbong tuff ring in that it shows the characteristics of an alkali magma batch forming a tuff cone and a sub-alkali magma batch forming subsequent lavas. The two magmas of Udo did not erupt at the same time; but the subalkali magma erupted through the same single-dyke plumbing system after the alkali magma was completely exhausted. This is a seemingly simple, monogenetic volcano; however, it is an example of chemical and petrochemical diversity. The Suwolbong tuff ring is chemically similar to Udo; therefore, it was previously thought

to have experienced a fractionation regime similar to that of alkaline and sub-alkaline magmas (Brenna et al., 2010). However, the results of our study show that they experienced a fractionation regime that was different from that of Udo.

The confusion between juvenile and accidental materials in volcaniclastic deposits can result in incorrect interpretations of the magma properties, the magma plumbing system, and the eruption styles, eventually leading to wrong prediction of future volcanic eruptions and related volcanic hazards.

## 7. CONCLUSIONS

The glassy pyroclasts of the Suwolbong tuff ring, Jeju Island, Korea, were found to comprise both juvenile and accidental particles, necessitating reinterpretation of the magma plumbing system of the volcano. Based on the particle texture and geochemical composition, the glassy pyroclasts could be divided into vesicular and unaltered and non-vesicular and altered particles. The former are alkaline in composition, volumetrically abundant (avg. 35 vol%), and show a vesicularity change in relation to the lithofacies change in the outcrop. In contrast, the latter is alkaline to subalkaline in composition and less abundant (avg. 8 vol%) in the deposits, and show alteration rims along the particle margins. These features indicate that they were accidentally derived from the underlying volcaniclastic strata. Subalkali hyaloclastite layers in the subsurface are interpreted to have been the sources of the accidental glassy particles. Based only on the geochemical characteristics of the newly defined juvenile glass, i.e., the vesicular alkaline glass, mainly containing olivine, clinopyroxene, and plagioclase, we interpret that the Suwolbong tuff ring formed from alkaline magmas that ascended through a rather simple magma-plumbing system in contrast to a previous model. The magma plumbing system of Suwolbong is inferred to have been fed by at least three independently ascending magma batches, which have been erupted in order from a single large dike system without interaction between them during the eruption.

This study suggests that proper distinction between juvenile and accidental particles is essential for accurately understanding the properties of the source magma and the magma plumbing system in phreatomagmatic monogenetic volcanoes, which commonly contain considerable amounts of accidental materials.

## ACKNOWLEDGMENTS

This study was funded by the Korea Institute of Geoscience and Mineral Resources (Principal Research Fund GP2021-006). We thank Dr. J. B. Park and Dr. Y. M. Jeon for constructive comments on the manuscript. Also, we sincerely appreciate the editor,

Y. B. Cheon, and the managing editor, B. K. Ko, for their careful review and feedback.

## REFERENCES

- Ahn, U.S., Sohn, Y.K., Yoon, W.S., Ryu, C.K., Jeong, J.O., and Kang, C.W., 2015, Geochemical fingerprinting of basaltic glass in tephra deposits underlying the human footprints-bearing strata in Jeju Island, Korea: provenance of tephra and age of the human footprints. *Journal of the Geological Society of Korea*, 51, 105–126. (in Korean with English abstract)
- Bamber, E.C., La Spina, G., Arzilli, F., Polacci, M., Mancini, L., de' Michieli Vitturi, M., Andronico, D., Corsaro, R.A., and Burton, M.R., 2024, Outgassing behaviour during highly explosive basaltic eruptions. *Communications Earth & Environment*, 5, 1–16.
- Barberi, F., Cioni, R., Rosi, M., Santacroce, R., Sbrana, A., and Vecchi, R., 1989, Magmatic and phreatomagmatic phases in explosive eruptions of Vesuvius as deduced by grain-size and component analysis of the pyroclastic deposits. *Journal of Volcanology and Geothermal Research*, 38, 287–307.
- Brenna, M., Cronin, S.J., Kereszturi, G., Sohn, Y.K., Smith, I.E., and Wijbrans, J., 2015, Intraplate volcanism influenced by distal subduction tectonics at Jeju Island, Republic of Korea. *Bulletin of Volcanology*, 77, 1–16.
- Brenna, M., Cronin, S.J., Nemeth, K., Smith, I.E., and Sohn, Y.K., 2011, The influence of magma plumbing complexity on monogenetic eruptions, Jeju Island, Korea. *Terra Nova*, 23, 70–75.
- Brenna, M., Cronin, S.J., Smith, I.E., Sohn, Y.K., and Németh, K., 2010, Mechanisms driving polymagmatic activity at a monogenetic volcano, Udo, Jeju Island, South Korea. *Contributions to Mineralogy and Petrology*, 160, 931–950.
- Cas, R.F. and Wright, J.V., 1987, *Volcanic Successions: Modern and Ancient*. Allen & Unwin, London, UK, 528 p.
- Cheong, C., Choi, J., Sohn, Y., Kim, J., and Jeong, G., 2007, Optical dating of hydromagmatic volcanoes on the southwestern coast of Jeju Island, Korea. *Quaternary Geochronology*, 2, 266–271.
- Cho, H.S., Lee, J.S., Lee, S.B., Kim, J.W., and Kim, T.J., 2021, Development of identification method of a volcanic crater based on magnetic approaches. Report, Korea Institute of Geoscience and Mineral Resources, Daejeon, South Korea, 75 p. (in Korean with English abstract) <http://library.kigam.re.kr/Search/Detail/62514> [Accessed on 13 May 2024].
- Del Gaudio, P., Mollo, S., Ventura, G., Iezzi, G., Taddeucci, J., and Cavallo, A., 2010, Cooling rate-induced differentiation in anhydrous and hydrous basalts at 500 MPa: implications for the storage and transport of magmas in dikes. *Chemical Geology*, 270, 164–178.
- Elliott, H., Gernon, T., Roberts, S., and Hewson, C., 2015, Basaltic maar-diatreme volcanism in the Lower Carboniferous of the Limerick Basin (SW Ireland). *Bulletin of Volcanology*, 77, 1–22.
- Fisher, R.V. and Schmincke, H.U., 1984, *Pyroclastic Rocks*. Springer-Verlag, Berlin, Germany, 472 p.
- Geshi, N., Németh, K., and Oikawa, T., 2011, Growth of phreatomagmatic explosion craters: a model inferred from Suoana crater in Miyakejima Volcano, Japan. *Journal of Volcanology and Geothermal Research*, 201, 30–38.
- Go, S.Y., Kim, G.B., Jeong, J.O., and Sohn, Y.K., 2017, Diatreme evolution during the phreatomagmatic eruption of the Songaksan tuff ring, Jeju Island, Korea. *Bulletin of Volcanology*, 79, 1–26.
- Graettinger, A., Valentine, G., and Sonder, I., 2016, Recycling in debris-filled volcanic vents. *Geology*, 44, 811–814.
- Hahn, J., Lee, Y., Kim, N., Hahn, C., and Lee, S., 1997, The groundwater resources and sustainable yield of Cheju volcanic island, Korea. *Environmental Geology*, 33, 43–53.
- Helz, R.T. and Thornber, C.R., 1987, Geothermometry of Kilauea Iki lava lake, Hawaii. *Bulletin of Volcanology*, 49, 651–668.
- Houghton, B. and Wilson, C., 1989, A vesicularity index for pyroclastic deposits. *Bulletin of Volcanology*, 51, 451–462.
- Indriyanto, J.N., Ohba, T., Hoshide, T., Angkasa, S.S., and Abdurrachman, M., 2023, Eruptive history of the last-1300-years activity of Kelud volcano, Indonesia: inferences from stratigraphy, chronology, sedimentology, componentry, and geochemistry. *Journal of Volcanology and Geothermal Research*, 433, 1–20.
- Jeon, Y.M., Park, K.H., and Sohn, Y.K., 2022, Hydrovolcanic activity on a continental shelf inferred from the subsurface diatreme-and crater-filling deposits of Jeju Island, Korea. *Bulletin of Volcanology*, 84, 1–24.
- Jeong, G.Y. and Sohn, Y. K., 2011, Microtextures, microchemistry, and mineralogy of basaltic glass alteration, Jeju Island, Korea, with implications for elemental behavior. *American Mineralogist*, 96, 1129–1147.
- Johnson, E.R., Wallace, P.J., Cashman, K.V., and Granados, H.D., 2010, Degassing of volatiles ( $\text{H}_2\text{O}$ ,  $\text{CO}_2$ , S, Cl) during ascent, crystallization, and eruption at mafic monogenetic volcanoes in central Mexico. *Journal of Volcanology and Geothermal Research*, 197, 225–238.
- Johnson, E.R., Wallace, P.J., Cashman, K.V., Granados, H.D., and Kent, A.J., 2008, Magmatic volatile contents and degassing-induced crystallization at Volcán Jorullo, Mexico: implications for melt evolution and the plumbing systems of monogenetic volcanoes. *Earth and Planetary Science Letters*, 269, 478–487.
- Koh, C.S., Yoon, S.H., Hong, J.G., Jeong, J.O., and Kim, J.J., 2019, Stratigraphic analysis of the drilling core in Woljong-ri coastal area, Jeju Island. *Journal of the Geological Society of Korea*, 55, 1–20. (in Korean with English abstract)
- Koh, C.S., Yoon, S.H., Hwang, S.H., and Shin, J.H., 2020, Origin and characteristics of glassy breccias from the boreholes in the Woljeong-Haengwon area of northeastern Jeju Island, Korea. *Journal of the Geological Society of Korea*, 56, 17–29. (in Korean with English abstract)
- Koh, G.W., 1997, Characteristics of the groundwater and hydrogeologic implications of the Seoguipo Formation in Cheju Island. Ph. D. Thesis, Pusan National University, Pusan, South Korea, 326 p. (in Korean with English abstract)
- Koh, G.W., Koh, C.S., Park, J.B., and Moon, D.C., 2015, Interpretation of the volcano growth under the sea level based on distribution of hyaloclastite breccia deposits in the subsurface of Jeju Island, Korea. Fall Joint Conference of Geological Science of Korea (Abstract), Jeju, Korea, Oct. 28–31, p. 86.
- Koh, G.W., Park, J.B., Kang, B.R., and Moon, D.C., 2013, Volcanism in Jeju Island. *Journal of the Geological Society of Korea*, 49, 209–230.

- (in Korean with English abstract)
- Lee, S.H., 2008, Characteristics of hydrogeological and groundwater occurrence in the western coastal areas of Jeju Island, Korea. MSc Thesis, Cheju National University, Jeju, South Korea, 95 p. (in Korean with English abstract)
- Lefebvre, N., White, J., and Kjarsgaard, B., 2013, Unbedded diatreme deposits reveal maar-diatreme-forming eruptive processes: Standing Rocks West, Hopi Buttes, Navajo Nation, USA. *Bulletin of Volcanology*, 75, 1–17.
- Lim, J., Lee, J.Y., Kim, J.C., Hong, S.S., and Choi, H., 2015, Paleoenvironmental and volcanologic implications of the Gosan Formation in Jeju Island, Korea. *Journal of the Geological Society of Korea*, 51, 537–544. (in Korean with English abstract)
- Lorenz, V., 1986, On the growth of maars and diatremes and its relevance to the formation of tuff rings. *Bulletin of Volcanology*, 48, 265–274.
- Luhr, J.F., 2001, Glass inclusions and melt volatile contents at Paricutin Volcano, Mexico. *Contributions to Mineralogy and Petrology*, 142, 261–283.
- Mair, A., Hagedorn, B., Tillery, S., El-Kadi, A.I., Westenbroek, S., Ha, K., and Koh, G.W., 2013, Temporal and spatial variability of groundwater recharge on Jeju Island, Korea. *Journal of Hydrology*, 501, 213–226.
- McPhie, J., Doyle, M., and Allen, R., 1993, Volcanic textures: a guide to the interpretation of textures in volcanic rocks. Centre for Ore Deposit and Exploration Studies, University of Tasmania, Hobart, Australia, 198 p.
- Murtagh, R.M. and White, J.D., 2013, Pyroclast characteristics of a subaqueous to emergent Surtseyan eruption, Black Point volcano, California. *Journal of Volcanology and Geothermal Research*, 267, 75–91.
- Murtagh, R.M., White, J.D., and Sohn, Y.K., 2011, Pyroclast textures of the Ilchulbong ‘wet’ tuff cone, Jeju Island, South Korea. *Journal of Volcanology and Geothermal Research*, 201, 385–396.
- Németh, K. and Martin, U., 2007, Shallow sill and dyke complex in western Hungary as a possible feeding system of phreatomagmatic volcanoes in “soft-rock” environment. *Journal of Volcanology and Geothermal Research*, 159, 138–152.
- Németh, K., Martin, U., and Harangi, S., 2001, Miocene phreatomagmatic volcanism at Tihany (Pannonian Basin, Hungary). *Journal of Volcanology and Geothermal Research*, 111, 111–135.
- Okumura, S., Nakamura, M., Takeuchi, S., Tsuchiyama, A., Nakano, T., and Uesugi, K., 2009, Magma deformation may induce non-explosive volcanism via degassing through bubble networks. *Earth and Planetary Science Letters*, 281, 267–274.
- Park, J., Park, K., Cho, D., and Koh, G., 1999, Petrochemical classification of the Quaternary volcanic rocks in Jeju Island, Korea. *Journal of Geological Society of Korea*, 35, 253–264. (in Korean with English abstract)
- Park, K., Lee, B., Kim, J., Cho, D., Lee, S., Choi, H., Park, D., Lee, S., Choi, Y., and Yang, D., 2000, Explanatory note of the Jeju (Baekado, Jinnampo) sheet (1: 250,000). Korea Institute of Geoscience and Mineral Resources, Daejeon, Sout Korea, 59 p. (in Korean with English abstract)
- Polacci, M., Baker, D.R., Bai, L., and Mancini, L., 2008, Large vesicles record pathways of degassing at basaltic volcanoes. *Bulletin of Volcanology*, 70, 1023–1029.
- Romero, J.E., Ureta, G., Fuentes, P., Corgne, A., Naranjo, J.A., Ramirez, C.F., Chako-Tchamabe, B., Caceres, M., and Lazcano, J., 2022, The eruptive history and magma composition of Pleistocene Cerro Negro volcano (Northern Chile): implications for the complex evolution of large monogenetic volcanoes. *Journal of Volcanology and Geothermal Research*, 429, 1–20.
- Ross, P.S., White, J.D., Zimanowski, B., and Büttner, R., 2008a, Multiphase flow above explosion sites in debris-filled volcanic vents: insights from analogue experiments. *Journal of Volcanology and Geothermal Research*, 178, 104–112.
- Ross, P.S., White, J.D., Zimanowski, B., and Büttner, R., 2008b, Rapid injection of particles and gas into non-fluidized granular material, and some volcanological implications. *Bulletin of Volcanology*, 70, 1151–1168.
- Schipper, C.I., White, J.D., Nichols, A.R., Burgisser, A., Hellebrand, E., and Murtagh, R.M., 2012, Incipient melt segregation as preserved in subaqueous pyroclasts. *Geology*, 40, 355–358.
- Smellie, J.L. and Edwards, B.R., 2016, Glaciovolcanism on Earth and Mars: Products, Processes, and Palaeoenvironmental Significance. Cambridge University Press, Cambridge, UK, 483 p.
- Smith, I. and Németh, K., 2017, Source to surface model of monogenetic volcanism: a critical review. In: Németh, K., Carrasco-Núñez, G., Aranda-Gómez, J.J., and Smith, I.E. (eds.), Monogenetic Volcanism. Geological Society, London, Special Publications, 446, p. 1–28. <https://doi.org/10.1144/SP446.14>
- Sohn, Y.K., 1996, Hydrovolcanic processes forming basaltic tuff rings and cones on Jeju Island, Korea. *Geological Society of America Bulletin*, 108, 1199–1211.
- Sohn, Y.K. and Chough, S.K., 1989, Depositional processes of the Suwolbong tuff ring, Jeju Island (Korea). *Sedimentology*, 36, 837–855.
- Sohn, Y.K., Park, J.B., Khim, B., Park, K.H., and Koh, G.W., 2002, Stratigraphy, petrochemistry and Quaternary depositional record of the Songaksan tuff ring, Jeju Island, Korea. *Journal of Volcanology and Geothermal Research*, 119, 1–20.
- Sohn, Y.K. and Park, K.H., 2004, Early-stage volcanism and sedimentation of Jeju Island revealed by the Sagye borehole, SW Jeju Island, Korea. *Geosciences Journal*, 8, 73–84.
- Sohn, Y.K., Park, K.H., and Yoon, S.H., 2008, Primary versus secondary and subaerial versus submarine hydrovolcanic deposits in the subsurface of Jeju Island, Korea. *Sedimentology*, 55, 899–924.
- Sweeney, M.R. and Valentine, G.A., 2015, Transport and mixing dynamics from explosions in debris-filled volcanic conduits: numerical results and implications for maar-diatreme volcanoes. *Earth and Planetary Science Letters*, 425, 64–76.
- Taddeucci, J., Pomilio, M., and Scarlato, P., 2004, Conduit processes during the July–August 2001 explosive activity of Mt. Etna (Italy): inferences from glass chemistry and crystal size distribution of ash particles. *Journal of Volcanology and Geothermal Research*, 137, 33–54.
- Valentine, G.A. and Connor, C.B., 2015, Basaltic volcanic fields. In: Sigurdsson, H., Houghton, B., McNutt, S.R., Rymer, H., and Stix, J. (eds.), Encyclopaedia of Volcanoes (2nd edition). Academic Press,

- London, UK, p. 423–439. <https://doi.org/10.1016/B978-0-12-385938-9.00023-7>
- Valentine, G.A., Graettinger, A.H., Macorps, É., Ross, P.S., White, J.D., Döhring, E., and Sonder, I., 2015, Experiments with vertically and laterally migrating subsurface explosions with applications to the geology of phreatomagmatic and hydrothermal explosion craters and diatremes. *Bulletin of Volcanology*, 77, 1–17.
- Valentine, G.A. and Krogh, K.E., 2006, Emplacement of shallow dikes and sills beneath a small basaltic volcanic center – the role of pre-existing structure (Paiute Ridge, southern Nevada, USA). *Earth and Planetary Science Letters*, 246, 217–230.
- Valentine, G.A., Shufelt, N.L., and Hintz, A.R., 2011, Models of maar volcanoes, Lunar crater (Nevada, USA). *Bulletin of Volcanology*, 73, 753–765.
- Valentine, G.A. and White, J.D., 2012, Revised conceptual model for maar-diatremes: subsurface processes, energetics, and eruptive products. *Geology*, 40, 1111–1114.
- Valentine, G.A., White, J.D., Ross, P.S., Graettinger, A.H., and Sonder, I., 2017, Updates to concepts on phreatomagmatic maar-diatremes and their pyroclastic deposits. *Frontiers in Earth Science*, 5. <https://doi.org/10.3389/feart.2017.00068>
- Walker, G.P., 1993, Basaltic-volcano systems. In: Prichard, H.M., Alabaster, T., Harris, N.B.W., and Neary, C.R. (eds.), *Magmatic Processes and Plate Tectonics*. Geological Society, London, Special Publications, 76, p. 3–38. <https://doi.org/10.1144/GSL.SP.1993.076.01.01>
- White, J.D., 1996, Pre-emergent construction of a lacustrine basaltic volcano, Pahvant Butte, Utah (USA). *Bulletin of Volcanology*, 58, 249–262.
- White, J.D. and Houghton, B., 2000, Surtseyan and related phreatomagmatic eruptions. In: Sigurdsson, H., Houghton, B., McNutt, S.R., Rymer, H., and Stix, J. (eds.), *Encyclopedia of Volcanoes*. Academic Press, San Diego, USA, p. 495–511.
- White, J.D. and Ross, P., 2011, Maar-diatreme volcanoes: a review. *Journal of Volcanology and Geothermal Research*, 201, 1–29.
- Won, J.H., Kim, J.W., Koh, G.W., and Lee, J.Y., 2005, Evaluation of hydrogeological characteristics in Jeju Island, Korea. *Geosciences Journal*, 9, 33–46.
- Won, J.H., Lee, J.Y., Kim, J.W., and Koh, G.W., 2006, Groundwater occurrence on Jeju Island, Korea. *Hydrogeology Journal*, 14, 532–547.
- Woo, K.S., Sohn, Y.K., Yoon, S.H., Ahn, U.S., and Spate, A., 2013, *Jeju Island Geopark - A Volcanic Wonder of Korea*. Springer, Berlin, Germany, 88 p.

**Publisher's Note** Springer Nature remains neutral with regard to jurisdictional claims in published maps and institutional affiliations.